# Development of Tropical Cyclones from Mesoscale Convective Systems

by

Marja Helena Bister

Filosofian kandidaatti, Meteorology (1991)

University of Helsinki

Submitted to the Department of Earth, Atmospheric and Planetary Sciences in Partial Fulfillment of the Requirements for the Degree of

DOCTOR OF PHILOSOPHY IN METEOROLOGY

at the

MASSACHUSETTS INSTITUTE OF TECHNOLOGY

June 1996



Author .....
Department of Earth, Atmospheric and Planetary Sciences
March 29, 1996

Certified by .....
Kerry A. Emanuel
Professor of Meteorology
Thesis Supervisor

Accepted by .....
Thomas H. Jordan
Department Head

# Development of Tropical Cyclones from Mesoscale Convective Systems

by

Marja Bister

Submitted to the Department of Earth, Atmospheric and Planetary Sciences on March 29, 1996 in partial fulfillment of the requirements for the degree of Doctor of Philosophy in Meteorology

## Abstract

Hurricanes do not develop from infinitely small disturbances. It has been suggested that this is because of the effect of downdrafts on boundary layer $\Theta_e$. The goal of this work is to understand what kind of initial disturbances can induce tropical cyclogenesis. Data from a mesoscale convective system (MCS) that developed into hurricane Guillermo in 1991, were analysed. The MCS was an object of intensive observations during Tropical Experiment in Mexico. Data were collected using two aircraft flying into the MCS every 14 hours. A vortex, strongest in the middle troposphere, with a lower tropospheric humid and cold core, was found in the stratiform precipitation region of the MCS. A negative anomaly of virtual potential temperature and $\Theta_e$ in the boundary layer suggest that the cold anomaly was at least partially owing to evaporation of rain. A hurricane developed from the cold core vortex in about three days.

A nonhydrostatic axisymmetric model by Rotunno and Emanuel was used to study whether evaporation of precipitation from a prescribed mesoscale showerhead could lead to a vortex with a lower tropospheric humid and cold core. In the model this indeed happens and the cold core vortex develops into a hurricane. If the showerhead precipitation is weak and stopped too early, the vortex that develops as a result of evaporation barely extends to the boundary layer, and the system barely develops into a hurricane. This suggests that without external forcing, a cold core vortex that does not extend to the boundary layer does not develop into a hurricane. Further experiments were made to test whether the cold core vortex itself or the associated high relative humidity is more important for cyclogenesis. In the model, high relative humidity can make cyclogenesis occur two days earlier, but without the vortex does not lead to cyclogenesis. The cold core favors shallow convection even in the presence of negative anomaly of $\Theta_e$ in the boundary layer, thereby reducing the negative effects of downdrafts when the wind speed is still small.

A simple thought experiment suggests that evaporation lasting for less than the time it takes parcels to descend through the layer experiencing evaporation leads to a cyclone with an anticyclone below it. This idea is supported by numerical simulations. The thought experiment also suggests that relative flow through the system can prevent downward development of the vortex or even its formation. The prevention of the downward propagation of the vortex could be one reason for the observed negative effect of shear on tropical cyclogenesis. Composite analysis of tropical cyclogenesis over western Pacific by Zehr supports the important role of the cold core vortex extending all the way to the boundary layer.

Thesis Supervisor: Kerry A. Emanuel
Title: Professor of Meteorology

# Acknowledgements

I thank my thesis advisor, Kerry Emanuel, for his guidance, constructive criticism, and going carefully over several drafts of this thesis. I have benefitted greatly from discussions with him on scientific problems within and outside of hurricane research. I would like to thank John Marshall, Dave Raymond from New Mexico Institute of Mining and Technology, and Earle Williams for serving in my thesis committee, reading the thesis, and suggesting many improvements to it. I am also grateful to Jochem Marotzke, Richard Rosen and Peter Stone for serving in my thesis committee at the early stage of my studies.

I am grateful to several people outside of MIT who contributed to this work. Bob Burpee and Stan Rosenthal gave me the opportunity to work at the Hurricane Research Division of NOAA, where I edited the Doppler wind fields. Frank Marks and John Gamache helped me use the software at the Hurricane Research Division. Richard Rotunno of National Center for Atmospheric Research helped me with my questions about the Rotunno-Emanuel model.

I benefitted from scientific discussions with many students, particularly Michael Morgan, Nilton Rennò, and Lars Schade. I thank Françoise Robe for discussions related to coursework and our tropical research topics, and especially for her friendship.

Jane McNabb, Joel Sloman, and Tracey Stanelun helped coping with bureaucracy.

I thank my father Martti and my sisters Liisa and Anja for their love and support. Martti's encouragement and his example as a scientist have been crucial. I thank my husband Esko Keski-Vakkuri for his love and imagination.

I dedicate this thesis to the memory of my mother, Anna-Liisa.

# Table of Contents

# List of Figures

# List of Tables

# Chapter 1

# Introduction

Riehl (1954) noted that tropical cyclones do not form spontaneously, but from disturbances of independent dynamical origin. Tropical cyclones have often been observed to be triggered by easterly waves (e.g. Shapiro 1977). But only about one out of ten easterly waves develops into a hurricane (Avila 1991). Shapiro (1977) noted that the development of some easterly waves into tropical cyclones may depend on the characteristics of the mean flow. On the other hand, it has been suggested that upper tropospheric potential vorticity (PV) anomalies could trigger cyclogenesis. Simpson and Riehl (1981) discuss several cases of tropical cyclogenesis that are associated with an approaching upper tropospheric trough. However, they also note that in some cases an upper tropospheric trough seems to cause an incipient storm to die. Reilly (1992) studied tropical cyclogenesis over western North Pacific in summer 1991, and noted that majority of the cases were associated with positive advection of PV in the upper troposphere. Montgomery and Farrell (1993) have studied the effect of an upper tropospheric PV anomaly on a weak surface cyclone using a balanced model. Their results suggest that an upper tropospheric PV anomaly moving with respect to the lower level winds might result in a spin-up of a weak surface cyclone. Molinari et al. (1995) studied intensification of hurricane Emily associated with an upper tropospheric PV anomaly. Their results suggest that tropical cyclones can intensify as a result of vertical alignment of an upper tropospheric PV anomaly and the cyclone in the lower troposphere. However, they stress that a large-scale upper tropospheric PV anomaly would be associated with vertical shear strong enough so that weakening of the cyclone would result. They view the upper tropospheric anticyclone associated with the tropical cyclone important in reducing the scale of the approaching

upper tropospheric PV anomaly so that shear associated with the upper tropospheric PV anomaly is small. However, it is still not known how important in practice the upper tropospheric PV anomalies are for cyclogenesis, and what the exact mechanism of the possible cyclogenesis associated with these PV anomalies is.

There have been several studies of tropical cyclogenesis using numerical models. However, as noted by Rotunno and Emanuel (1987), in none of the simulations has the model's initial state been neutral to convection. Large available energy for convection has lead to a rapid intensification of very weak perturbations in the wind field (e.g. in the model of Anthes 1972), which is not consistent with the observation that tropical cyclones do not form in the absence of disturbances of independent dynamical origin. Rotunno and Emanuel (1987) studied the nature of tropical cyclogenesis using a model with an initial state that is neutral to model's convection. Their study will be discussed in section 1.1.

In this work I study the problem of tropical cyclogenesis from **mesoscale** perspective. The results of this work suggest that a long-lasting mesoscale convective system can induce tropical cyclogenesis. More specifically, evaporation of mesoscale precipitation that lasts long enough and is associated with little shear (or more generally, little relative flow through the precipitation region) can lead to a formation of a hurricane. Two important questions that are not addressed in this study are: 1) What is the mechanism behind the formation and maintenance of long-lived mesoscale convective systems? 2) Is there a relation between upper tropospheric PV anomalies and mesoscale convective systems?

## 1.1 Tropical Experiment in Mexico (TEXMEX) and hurricane Guillermo

The fact that tropical cyclones develop from disturbances of independent dynamical origin leads to two questions: Why do not tropical cyclones form spontaneously? What kind of initial disturbances can induce tropical cyclogenesis, and how do they form? Rotunno and Emanuel (1987, hereinafter RE) and Emanuel (1989) attempted to answer the first question. Results from their numerical simulations suggest that convective downdrafts bring air of low equivalent potential temperature ($\theta_e$) into the boundary layer, preventing further convection. Therefore, for tropical cyclogenesis to occur, the negative effect of the downdrafts has to be overcome. In principle this might happen owing to an increase of $\theta_e$ in the middle troposphere, an increase of relative humidity so that evaporation of rain does not occur, or an increase of wind speed so that the sea surface fluxes keep replenishing the boundary layer $\theta_e$. Indeed, Emanuel et al. (1994) claim that convection, in quasi-equilibrium with forcing, can cause positive temperature anomalies only if it is associated with a positive anomaly of sea surface temperature, surface wind speed, or $\theta_e$ above the subcloud layer, or a negative anomaly in convective downdraft mass flux. The simulations by RE and Emanuel (1989), in which a warm core vortex was used in the initial state, suggested that an increase of $\theta_e$ in the middle troposphere is needed for tropical cyclogenesis to be possible. The main goal of TEXMEX, a field experiment to study tropical cyclogenesis over eastern North Pacific, was to test a hypothesis stated in the TEXMEX Operations Plan (Emanuel 1991): The elevation of $\theta_e$ in the middle troposphere just above a near-surface vorticity maximum is a necessary and perhaps sufficient condition for tropical cyclogenesis. It was assumed that the elevation of $\theta_e$ is accomplished by deep convection bringing high $\theta_e$ to the middle troposphere, as occurs in the models initialized by warm core vortices. Analysis of one of the TEXMEX cases, a mesoscale convective system that

developed into hurricane Guillermo, showed a moderate increase of $\theta_e$ at 3 km altitude. The value of $\theta_e$ remained constant, however, for over a day before rapid strengthening started, suggesting that the observed increase of midtropospheric $\theta_e$ was not enough to start the intensification. Concerning the TEXMEX hypothesis, the role of downdrafts had certainly been diminished owing to the positive anomaly of $\theta_e$ and relative humidity in the initial vortex. But since the increase of midtropospheric $\theta_e$ was not enough to start the intensification it is clear that in this case the increase of $\theta_e$ is not a sufficient condition for tropical cyclogenesis.

The goal of this work is to answer the second question posed on tropical cyclogenesis. What kind of initial disturbances can induce tropical cyclogenesis, and how do they form? The basis for this study are the observations made in the disturbance that developed into tropical cyclone Guillermo. The initial perturbation was found in a mesoscale convective system (MCS). Houze (1993, p. 334) defines an MCS as a cloud system that occurs in connection with an ensemble of thunderstorms and produces a contiguous precipitation area of 100 km or more in horizontal scale in at least one direction. MCSs typically last from hours to days, and consist of deep convective clouds, and a stratiform precipitation region. The stratiform precipitation falls from an anvil cloud. The anvil cloud consists in part of debris from deep convective clouds. There is also condensation in the anvil cloud that increases the stratiform precipitation. The depth of the anvil cloud varies, but the base is often close to the isotherm of 0 C, that resides near 5 km altitude.

The disturbance that developed into hurricane Guillermo was very different from the warm core disturbance used in the initial state in the simulations on which the TEXMEX hypothesis was based. A vortex, with cyclonic wind increasing with height in the lower troposphere, was found in the stratiform precipitation region of the MCS. The vortex had a cold core in the lower troposphere. At 3 km altitude relative humidity was anomalously

high. The data from the pre-Guillermo mesoscale system were collected over a period of 3 days. The humid cold core vortex existed already at the time of the first flight. A warm core system developed within the cold core and intensified into a hurricane during the period of intensive observations. To our knowledge, this is the best data set documenting the development of a weak lower tropospheric cold core vortex into a hurricane.

## 1.2 Previous work on tropical cyclogenesis from mesoscale systems

The understanding of tropical cyclogenesis has traditionally meant the understanding of the increase of **vorticity**. A positive anomaly in vorticity is associated with increased sea surface fluxes owing to higher wind speed, and a decreased Rossby radius of deformation (e.g. Chen and Frank 1993). The former enhances convection, and the latter increases the local increase of temperature associated with convection. The role of **relative humidity** has been less studied, perhaps due to the observation that midtropospheric relative humidities do not differ in large-scale environments of convective systems which intensify into hurricanes and those which do not (McBride and Zehr 1981). Tropical disturbances that develop into named storms have been observed to exist in an environment of very weak **vertical wind shear** (Gray 1968). The negative effect of vertical wind shear has often been explained by "ventilation". Heating associated with deep convection is said to be advected away from the disturbance if vertical shear is large (with vertical shear the whole storm cannot move with the mean wind). Another effect of vertical wind shear could be the tilting of the potential vorticity anomaly associated with the storm (Jones 1995).

Based on these climatological aspects of cyclogenesis, it has been natural that studies aiming at understanding tropical cyclogenesis have concentrated in the formation of vorticity. It has been argued that vorticity associated with easterly waves might be conducive to cyclogenesis. Indeed, tropical cyclogenesis over the eastern Pacific is often associated

with easterly waves (Miller, 1991). As discussed before, the second possible source for vorticity is upper tropospheric potential vorticity anomalies. However, there was no evidence in the ECMWF data of independent upper tropospheric positive potential vorticity anomalies in the region where hurricane Guillermo formed (Molinari, personal communication 1996). The MCS from which hurricane Guillermo developed formed while an easterly wave was propagating into the eastern Pacific from the Caribbean Sea (Farfan and Zehnder, 1996, hereinafter FZ). The easterly wave and its interaction with topography may have been important factors in increasing vorticity initially, as suggested by FZ.

Early research into tropical cyclogenesis (see Handel 1990 for an extensive review) assumed that the increase of vorticity occurs owing to convergence into deep convection, and is associated with heating. Lately it has been recognized that vorticity production associated with convection usually takes place in the stratiform precipitation region of MCSs. Midtropospheric vortices have been observed in circular MCSs (e.g. Bartels and Maddox, 1991), and also in squall lines (e.g. Gamache and Houze, 1985). It has been suggested that these vortices may be due to vertical heating gradients in the stratiform precipitation region. On the other hand, results of numerical simulations of a squall line by Davis and Weisman (1994) suggest that line end vortices can form owing to horizontal heating gradients acting on initially horizontal vorticity. Chen and Frank (1993) simulated the formation of a midlevel vortex in a midlatitude MCS. In their model the development of a vortex occurs as a response to a vertical heating gradient in the presence of anomalously small local Rossby deformation radius. The small Rossby deformation radius is owing to decreased vertical stability in the anvil cloud. The decreased stability decreases the group speed of gravity waves, thereby preventing spatial dispersion of energy. Therefore, heating in the anvil could lead to a balanced vortex.

There is a relation between MCSs and tropical cyclogenesis. Both mesoscale convective complexes (Velasco and Fritsch, 1987) and tropical cyclones (Zehnder and Gall, 1991) are more frequent over the eastern North Pacific than in the Caribbean. There is also ample evidence in satellite imagery of mesoscale convective complexes leading to tropical cyclogenesis (e.g. Velasco and Fritsch, 1987 and Laing and Fritsch, 1993). In addition, there is in situ data of tropical cyclogenesis from mesoscale convective systems with a midlevel vortex. Bosart and Sanders (1981) studied a midlatitude MCS in which a midlevel vortex had developed. The vorticity extended to quite low altitudes but there was no evidence of surface circulation before the system was over the ocean. Later, over the ocean, the system developed into a storm resembling a tropical cyclone. Moreover, observations by Davidson et al. (1990) show that the AMEX tropical cyclones Irma and Jason initially had maximum intensity in the middle troposphere.

Since tropical cyclones have been observed to develop from MCSs with a midtropospheric vortex, the important question becomes how the midlevel vortex leads to a formation of low level vorticity. In Chen and Frank's study of the formation of a vortex in a midlatitude MCS, the midlevel vortex descends downward. They associate the downward movement of the midlevel vortex with the downward development of updraft and warm core in the stratiform rain region. By as early as 8 h of simulated time the warm core structure extends down to 850 hPa. This rapid downward extension of the warm core is unlike what was observed in the pre-Guillermo MCS, where it takes about two days for the warm core to develop in the lower troposphere. It must be noted that Chen and Frank's initial condition was characterized by a large value of CAPE and a very moist lower troposphere. It is unlikely that this kind of downward development could occur in an environment with a dry middle troposphere.

Mapes and Houze (1995) have noted that the downward development of the midlevel vortex could be a natural consequence of convection occurring in the region of the midlevel vortex. This idea is based on observations of divergence in a rainband of cyclone Oliver, 1993. Convection in the rainband adjusts itself to oppose temperature perturbations in the rainband, implying large convective heating in the cold region, and less heating above the cold region. The associated divergence would tend to increase vorticity close to the surface and decrease it above the cold core. However, they do not explain how convection would form in the region of the midlevel vortex. The downdraft, in the stratiform precipitation region, brings low $\Theta_e$ air to the boundary layer, which tends to prevent convection. It is important to explain how convection can ensue when $\Theta_e$ has a negative anomaly in the boundary layer.

## 1.3 Goals

The basis of TEXMEX was the prediction of numerical models that the downdrafts owing to evaporation of precipitation and detrainment of cloud are a key factor in preventing tropical cyclogenesis. Since the relative humidity of the initial system, as well as $\Theta_e$, was elevated, it was natural to assume that the effect of downdrafts on the boundary layer $\Theta_e$ would be minor, and that tropical cyclogenesis would be favored by these thermodynamic factors. Indeed, Emanuel (1995) has found that if a whole atmospheric column of 150 km in radius is saturated, a hurricane forms in a couple of days from an initial vortex with 3 $ms^{-1}$ maximum wind. On the other hand, earlier research has concentrated on the formation of the midlevel vortex and its downward development. And, as we have seen, there is plenty of evidence of tropical cyclones developing from MCSs with midlevel vortices.

The perturbation from which hurricane Guillermo developed was associated with both a cold core vortex and high relative humidity. The goal of this work is to shed light on the

following questions: How did the initial disturbance with a humid cold core vortex develop? How did the midlevel vortex descend downward? Is the existence of a humid cold core vortex, as observed in pre-Guillermo, a suitable initial disturbance for cyclogenesis? And if it turns out it is, is the high humidity or the vortex itself more important for cyclogenesis?

An overview of TEXMEX is given in Chapter 2. Also the sources of data, and analysis methods are discussed in Chapter 2. Results from the data analysis are presented in Chapter 3, in which the development of the pre-Guillermo disturbance into a hurricane is documented. The numerical model that I use to study the formation of the initial humid cold core vortex, and the relative importance of humidity and a cold core vortex, is described in Chapter 4. Chapters 5 and 6 contain results from the numerical simulations. In Chapter 5, results from simulations designed to improve our understanding of the formation of the initial humid cold core vortex, and its possible development into a hurricane are discussed. The relative importance of the humidity and the cold core vortex is addressed in Chapter 6.

The numerical simulations, presented in Chapter 5, suggest that a humid cold core vortex can be a result of evaporation of mesoscale precipitation, and that the vortex, formed in this way, is a suitable initial disturbance for tropical cyclogenesis. Results from Chapter 6 suggest that the vortex is more important for cyclogenesis than increased relative humidity. Sensitivity simulations suggest that if the vortex does not extend to the surface when the mesoscale precipitation ends, a hurricane will not form. In Chapter 7, a thought experiment that captures the crudest aspects of the downward propagation of a cold core cyclone is discussed. The thought experiment reveals some factors that affect the downward development, and gives a possible reason why vertical shear is unfavorable for tropical cyclogenesis. The likelihood that the mechanism for tropical cyclogenesis outlined in

this work would frequently be accountable for tropical cyclogenesis is discussed in light of observational work by Zehr (1976 and 1992) in Chapter 7. Chapter 8 contains concluding remarks.

# Chapter 2

# Data and analysis methods

In TEXMEX measurements were made inside developing and nondeveloping cloud clusters, using the WP-3D aircraft operated by the NOAA Office of Aircraft Operations (OAO) and the National Center for Atmospheric Research (NCAR) Lockheed Electra. Both aircraft were equipped to make in situ measurements of standard meteorological variables, and the WP-3D had the additional capability of deploying omega dropwinsondes and making detailed Doppler radar measurements. The aircraft measurement systems are described in detail in the TEXMEX Operations Plan (Emanuel 1991).

The eastern tropical North Pacific region was selected for the field program. This region has the highest frequency of genesis per unit area of any region worldwide (Elsberry et al., 1987). The field phase of the experiment began on 1 July and ended on 10 August 1991. During the project there were 6 Intensive Operation Periods (IOP's) that surveyed 1 short-lived convective system, 1 nondeveloping mesoscale cloud cluster, and 4 clusters that ultimately developed into hurricanes. The tracks of those systems that developed into hurricanes are shown in Fig. 2.1. Description of the aircraft flight operations are provided in the TEXMEX Data Summary (Rennó et al. 1992).

As the TEXMEX hypothesis concerned thermodynamic transformations of the lower and middle troposphere, most flight operations were conducted near the 700-hPa level and in the subcloud layer. Most of the NOAA WP-3D flights at 700 hPa deployed omega dropwinsondes, and the tail Doppler radar on the WP-3D operated almost uninterrupted through all of the flight operations. The aircraft flew alternating missions at approximately

14-hour intervals. Most flight missions lasted 7-9 hours, of which 1-3 hours were used in transit to the target area.

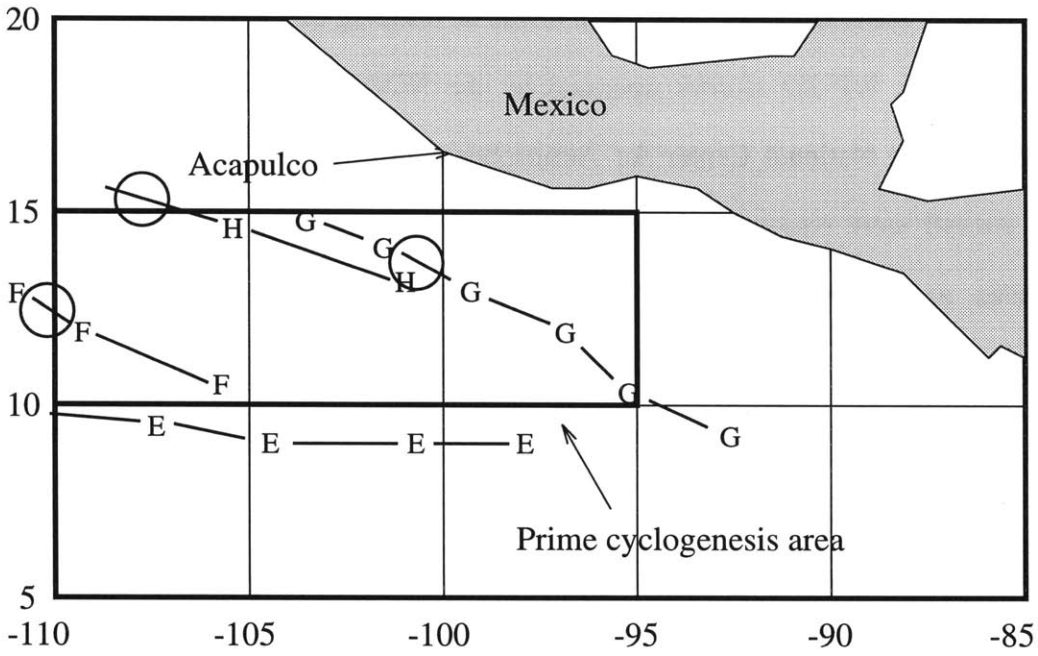


**Figure 2.1:** Tracks of aircraft-estimated vortex centers of TEXMEX cases that developed into hurricanes (D. Raymond, personal communication 1995). Circle shows where each disturbance was declared a tropical storm by National Hurricane Center. E is for Enrique, F for Fefa, G for Guillermo and H for Hilda.

The MCS that developed into hurricane Guillermo was chosen as the case study of this work because of the very good data coverage, and the very early state of the system during the first flight, as well as the interesting cold core structure of the storm. The MCS that developed into hurricane Guillermo on 5 August 1991 was the target object of IOP 5 from 2 August 1991 to 5 August 1991. Six flights were flown during IOP 5. The first, third, and fifth flights were flown with the Electra. These flights are labeled 1E, 3E, and 5E, respectively. The second, fourth, and sixth flights were flown with the WP-3D. These flights are

labeled 2P, 4P, and 6P, respectively. The flights are summarized in Table 2.1. Each flight consisted of several flight legs at 3 km altitude (700 hPa), and several more at 300 m. The first flight, 1E, was conducted well to the west of the developing system.

| Flight | Target | Date | Time at 700 hPa | Time at 300 m |
|---|---|---|---|---|
| 1E | - | 08/02/91 | - | - |
| 2P | pre-Guillermo | 08/02/91 | 01.19 -04.12 F | 04.19 - 06.10 F |
| 3E | pre-Guillermo | 08/03/91 | 15.10 - 18.10 | 18.24 - 19.30 |
| 4P | pre-Guillermo | 08/04/91 | 04.45 - 07.37 | 07.48 - 10.01 |
| 5E | TS Guillermo | 08/04/91 | 18.30 - 21.40 | 21.50 - 00.05 F |
| 6P | H Guillermo | 08/05/91 | 07.50 - 09.00 | 11.00 - 13.00 |

**Table 2.1: Summary of flights into (pre-)Guillermo. F is for following day, TS is for tropical storm, and H is for hurricane**

In the anvil precipitation the relative humidity measurements of the ODWs often showed 100% relative humidity, indicating wetting of instruments. Owing to the wetting, ODW data is not used in the data analysis. Radar composites from the WP-3D C-band radar, with antenna scanning in the horizontal plane, are used to get an overview of convection during the flights. Geostationary Operational Environmental Satellite (GOES) imagery and analysis of wind from the European Centre for Medium-Range Weather Forecasts (ECMWF) were obtained from Farfan and Zehnder of the University of Arizona.

## 2.1 Doppler radar data

### 2.1.1 Doppler radar and its operation

The characteristics of the WP-3D Doppler radar are given in Table 2.2. The unambiguous range and velocity are dictated by the pulse repetition frequency and the wavelength. The number of samples per each radar grid volume depends on the distance of the grid volume from the aircraft. There are at least 32 samples per each radar grid volume. The number of samples per grid volume increases with distance from the aircraft, being 128 for distances larger than 38.4 km.

| Radar characteristic | Value |
|---|---|
| Frequency | 9.315 GHz |
| Wavelength | 3.22 cm |
| Pulse length | 0.55 μs |
| Pulse repetition frequency | 1600 $s^{-1}$ |
| Beam width - along track | $1.35^0$ |
| Beam width - across track | $1.90^0$ |
| Unambiguous velocity | 12.88 $ms^{-1}$ |
| Unambiguous range | 93.75 km |

**Table 2.2: The characteristics of the NOAA WP-3D aircraft's Doppler radar.**

At least two beams from different angles are needed for the determination of the three dimensional wind. The usual method is to fly an L-pattern around the target object, keeping the antenna pointing angle perpendicular to the aircraft's ground track. This method has been used widely (e.g. Jorgensen et al. 1983, Marks and Houze 1984 and 1987). Another option is to use a Fore/Aft Scanning Technique (FAST). In FAST, the antenna tilt

angle, defined forward or aft from the perpendicular to the ground track, is changed between each rotation of the antenna about the aircraft's longitudinal axis. The WP-3D Doppler radar was operated using FAST in TEXMEX.

Since the antenna rotates at 10 RPM and the aircraft flies at a speed of 130 $ms^{-1}$, each revolution of the antenna in the same direction is separated by 1.6 km. The difference in time of two radials pointing to the same point at 80 km from the track is about 7 minutes. The difference is naturally much smaller than the one achieved by using the method of flying the L-pattern.

When FAST is used Doppler velocities are contaminated by the component of the velocity of the aircraft in the direction of the antenna. Thus, wind measurement is prone to errors in the aircraft's ground velocity. On the other hand, the FAST mode is practical when it is not possible to plan the flight pattern in advance. This is because the two components of the wind can be retrieved from one flight leg.

### 2.1.2 Editing

The Doppler data were mapped to a 3 x 3 x 0.5 km grid (0.5 km in the vertical direction) by averaging the data in the horizontal direction and interpolating in the vertical direction. The components of the aircraft's ground velocity and precipitation particle fallspeed in the direction of the antenna were subtracted from the radial velocities. Terminal fallspeed was estimated using empirical fallspeed - radar reflectivity relations for ice particles (Atlas et al. 1973) and for liquid water (Joss and Waldvogel 1970). These relations were also used by Marks and Houze (1987). The location of the radar bright band was used to determine where the precipitation was in the form of ice and where it was in the form of liquid. The depth of the bright band was estimated to be about 1.5 km. It was assumed that all precipitation was in the form of liquid below the bright band, and in the form of ice above it. In

the bright band region the two estimates were combined linearly.

The velocities were then unfolded automatically using Bargen and Brown's method (1980). An independent measure of the wind speed is needed to unfold the velocities. The in situ measurement of wind was used for this purpose. Manual editing of the data followed the automatic unfolding. Possible wrong unfolding was corrected for by adding a suitable number of unambiguous velocities (see Table 2.2) to any suspicious values. If the velocity still seemed unrealistic, the observation was deleted. Most of the deleting was done at 0.5, 1, and 1.5 km altitudes. Suspicious looking winds at higher altitudes were relatively rare, and probably owing to second or multiple trippers, or sidelobes. These errors will be discussed in section 2.1.3. Turning the aircraft in the middle of the flight leg also caused portions of the Doppler winds to be of poor quality, since the angle separation of the two radials was small. Fortunately, this problem occurred only once. The three-dimensional wind was calculated from the two radial components in the following way (the computer program was written by John Gamache of Hurricane Research Division/ NOAA): First, the horizontal wind components were calculated assuming that the vertical component is zero. Then, the horizontal components were used to calculate the first guess of the divergence field. Starting from the lowest level, the following procedure was repeated for each level until a prescribed accuracy was attained or until 50 iterations had been done. The vertical wind component for the first iteration was calculated from the anelastic continuity equation using vertical wind velocities from the level below, and the first guess estimate of divergence at the current level. Then, the three wind components were adjusted using the Least Squares method. The solution using this method usually converged to the desired accuracy in less than 50 iterations.

The data from separate flight legs had to be merged in a suitable way for the analysis of the whole MCS. To get a translation velocity of the system, the vortex center was

tracked from one flight to the next. This translation velocity was then used to move the data to appropriate locations at some reference time. If more than one datapoint was moved to the same gridvolume, an average was calculated. The data were mapped to a 5 x 5 x 0.5 km grid, 0.5 km being the vertical resolution. The possible evolution of the MCS while data were being collected was not accounted for. The MCS was long-lived, and the observed vortex within the MCS was at least qualitatively in balance with the mass field (see Chapter 3). Therefore, it is unlikely that there had been large changes in the mesoscale structure during the couple of hours that the aircraft flew in the MCS during each flight.

### 2.1.3 Error analysis

The across-track beamwidth (see Table 2.2) corresponds to 0.5, 1, and 2 km at ranges 15, 30, and 60 km, respectively. Thus, smearing of features is expected at large ranges. Note that the flight legs were typically about 60 km apart, and they were always parallel. Radar return from the sidelobes, $15^{o}$ from the center of the main lobe, can introduce errors to the data, especially in the region of sparse data and sea clutter. Sea clutter can affect the data far from the aircraft, and when the antenna is pointed downward. When the aircraft flies at 3 km altitude and the antenna is pointed horizontally the mainlobe of the beam will touch the sea surface at 90 km range. (The energy in the sidelobe can return from the sea surface from even smaller ranges, though.) The sea clutter contamination becomes a worse problem when the antenna is pointed downward. For example, when data are collected from an altitude of 1.5 km above the sea surface and the flight altitude is still 3 km the mainlobe touches the sea surface as close as 45 km from the aircraft. The Doppler velocities in the case studied were noisy below 2 km altitude. Where data from below 2 km was used in the analysis, care was taken that any suspicious-looking wind was deleted. In addition to sea

clutter and sidelobe problems, second and multitrippers, i.e. return coming form farther than the unambiguous range, can affect the data. Also, errors in terminal fallspeed estimates can affect the wind data.

Airborne radars have additional error sources compared to ground based radars. The error in the antenna pointing angles relative to the aircraft are smaller than $0.5^{o}$ (Marks, 1991 personal communication), and can be accounted for. The antenna position with respect to the ground is calculated using information of the aircraft attitude, given by the Inertial Navigation System. The aircraft attitude angles have errors less than $0.5^{o}$. The location and velocity of the aircraft are retrieved by integrating the accelerations given by the Inertial Navigation System. The ground velocity of the aircraft is subtracted from the Doppler velocities to eliminate the velocity component that is owing to the movement of the Doppler radar itself. Therefore, errors in the ground velocity will introduce errors in Doppler winds.

There is an independent source of wind data, which is the aircraft in situ measurement. The accuracy of the Doppler data is assessed by comparing the Doppler velocities to the in situ wind measurements. However, there are two types of errors that cannot be assessed by this comparison: those owing to errors in the ground speed of the aircraft and those owing to errors in terminal fallspeed estimates. First, when there is an error in the ground velocity of the aircraft, the associated error in the in situ wind is as large as in the Doppler wind since the in situ wind is calculated as a difference between true air speed and aircraft ground speed. Second, the error in the Doppler velocities due to errors in the estimated terminal fall speed of precipitation particles does not show up in the comparison, because when the antenna points horizontally, as it does when data is collected from the flight altitude, the component in the radial velocity due to terminal fallspeed is zero.

Merceret and Davis (1981) estimated the error in the ground speed to be at maximum 4 $ms^{-1}$. The error is now estimated to 2-3 $ms^{-1}$ (B. Damiano 1992, personal communication). The error introduced to Doppler velocities owing to an error in the ground speed is constant with height. Therefore, vertical differences of wind are not affected. Assuming an error of 1 $ms^{-1}$ in the terminal fallspeed (see Atlas et al.1973), the associated error in the horizontal wind speed for different ranges and elevation angles can be estimated. The errors are less than 1 $ms^{-1}$ for horizontal distances of more than 4 km from the flight track, assuming that no data farther than 4 km above or below the aircraft is used in the analysis. Moreover, for straight flight tracks this error is perpendicular to the flight track and shows up as spurious divergence or convergence.

The net effect of other errors than those associated with uncertainties in the ground speed and terminal fallspeed estimates is obtained in the following way: First a 3 km running mean of the in situ wind components was calculated. Then the values were linearly interpolated to those longitudes (latitudes, if leg happened to be oriented more in N-S direction) with gridded Doppler winds. The Doppler winds were then linearly interpolated to the latitudinal positions of the in situ winds. The mean differences and standard deviations were calculated for each flight separately. The results for the comparison of the in situ winds and Doppler winds merged from different flight legs are shown in Table 2.3. Note that some errors associated with the Doppler winds are expected to increase with distance from the aircraft. Therefore, a comparison of in situ wind and Doppler wind using only data from the particular flight track would not reveal these errors. However, when merged Doppler winds are used, Doppler data are usually a combination of data from different flight legs, even at the location of the flight track

The mean difference between in situ and merged Doppler wind components is always less than 2 $ms^{-1}$. However, the more interesting quantity is the standard deviation since it

is better related to the errors in the vorticity and divergence. The standard deviations are typically less than 2.5 $ms^{-1}$. However, for the boundary layer pattern of flight 4P the difference in the meridional component is 5.6 $ms^{-1}$. This most likely reflects a large error in the Doppler winds, as will be discussed in Chapter 3.

| Flight | Mean Δu | Mean Δv | SD Δu | SD Δv |
|---|---|---|---|---|
| 2P, 3 km flight pattern | -0.1 | -1.9 | 1.7 | 1.3 |
| 4P, 3 km flight pattern | 1.1 | 1.6 | 1.9 | 2.5 |
| 4P, 0.3 km flight pattern | -1.2 | 0.7 | 2.6 | 5.6 |
| 6P, 3 km flight pattern | 0.7 | -1.0 | 2.4 | 2.6 |

**Table 2.3: The mean and standard deviations of the differences between in situ and merged Doppler wind components**

In summary, the error in Doppler winds associated with the ground speed is at maximum 2-3 $ms^{-1}$. This error is constant with height, and does not affect vertical differences of wind. The errors associated with wrong estimates of terminal fallspeeds are less than 1 $ms^{-1}$ farther than 4 km from the flight track, and would mostly show up as spurious convergence of divergence. The other errors and their standard deviations are less than 2.5 $ms^{-1}$, except for the boundary layer pattern of flight 4P.

## 2.2 In situ data

Intercomparison of instruments onboard the NOAA WP-3D and the NCAR Electra was made using data from two sets of intercomparison flights in the beginning and at the end of the field experiment. The differences between the temperatures and the dew point temperatures measured by the two aircraft were less than 0.3 K both in the beginning and at

the end of the field experiment. These differences were accounted for, in the data analysis, by interpolating the differences in time and subtracting them from the data of the other aircraft.

Air that is part of an active convective updraft or downdraft should not be included in the thermodynamic analysis since air in updrafts and downdrafts is just passing through the altitude from which data were collected. Therefore, data were excluded if the magnitude of vertical velocity exceeded 1 $ms^{-1}$. Data were also excluded if the measured dew point temperature exceeded the measured temperature. However, no data were excluded from the 300 m analyses, nor were any data excluded from the analysis of thermodynamic fields from flight 6P, since the vertical velocity so often exceeded 1 $ms^{-1}$ during this flight. Using the same method as with the Doppler data, the data were renavigated to the appropriate locations at a given time, and 80-second (10 km) averages were calculated. These averages were then analyzed by hand.

# Chapter 3

# Analysis Results

The study by Farfan and Zehnder (1996) suggests that the easterly wave that was approaching the Eastern Pacific and its interaction with the Sierra Madre mountains increased vorticity in the vicinity of the MCS from which hurricane Guillermo formed. However, not all easterly waves lead to cyclogenesis. On the other hand, MCSs with midlevel vortices have been observed to lead to tropical cyclogenesis. The formation of a large and persistent MCS, even though possibly dependent on large-scale flow, might be enough to lead to tropical cyclogenesis. The analysis of data to be presented in this chapter will indeed justify pursuing the hypothesis that phase changes in the MCS may have been crucial for the formation of hurricane Guillermo. However, it is important to note the factors that contributed to the formation of the MCS are beyond the scope of this work and are left for future work.

## 3.1 Large-Scale Conditions

### 3.1.1 Satellite imagery

The mesoscale system developed over the Honduras-El Salvador border during the night of 1-2 August 1991. At 04 UTC on 2 August there is still practically no convection associated with it over the ocean. In Fig. 3.1a the infrared image from GOES is shown at 08 UTC on 2 August, 1991. At this time convection is spreading over the ocean and developing into a NNE-SSW oriented line extending southward from the coast. However, after a few hours the mesoscale system lost its line-like appearance (see Fig. 3.1 b and c). There is some suggestion in the satellite imagery of a convective line separating from the rest of

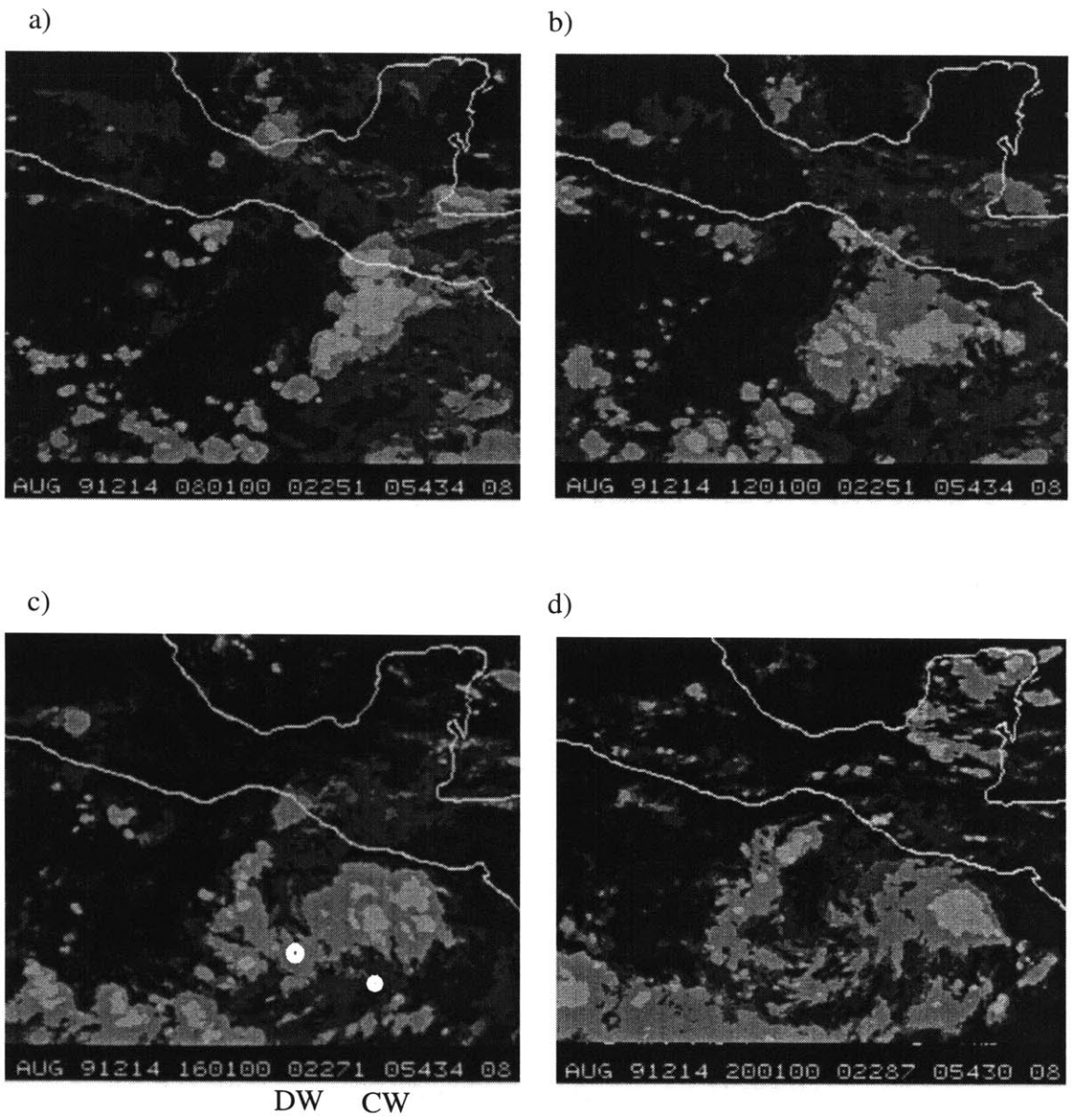


**Figure 3.1:** Infrared images from GOES at (a) 08 (b) 12 (c) 16 (d) and 20 UTC on 2 August 1991. In (c) the estimate of the location of the vortex center based on Doppler wind field is shown with letters DW, and the estimate based on cloud track wind field is shown with letters CW. The latter estimate is from FZ.

the MCS and propagating rapidly westward leaving the rest of the MCS behind (Figs. 3.1 c and d, and Fig. 3.2a). The convective line seems to weaken while the rest of the MCS

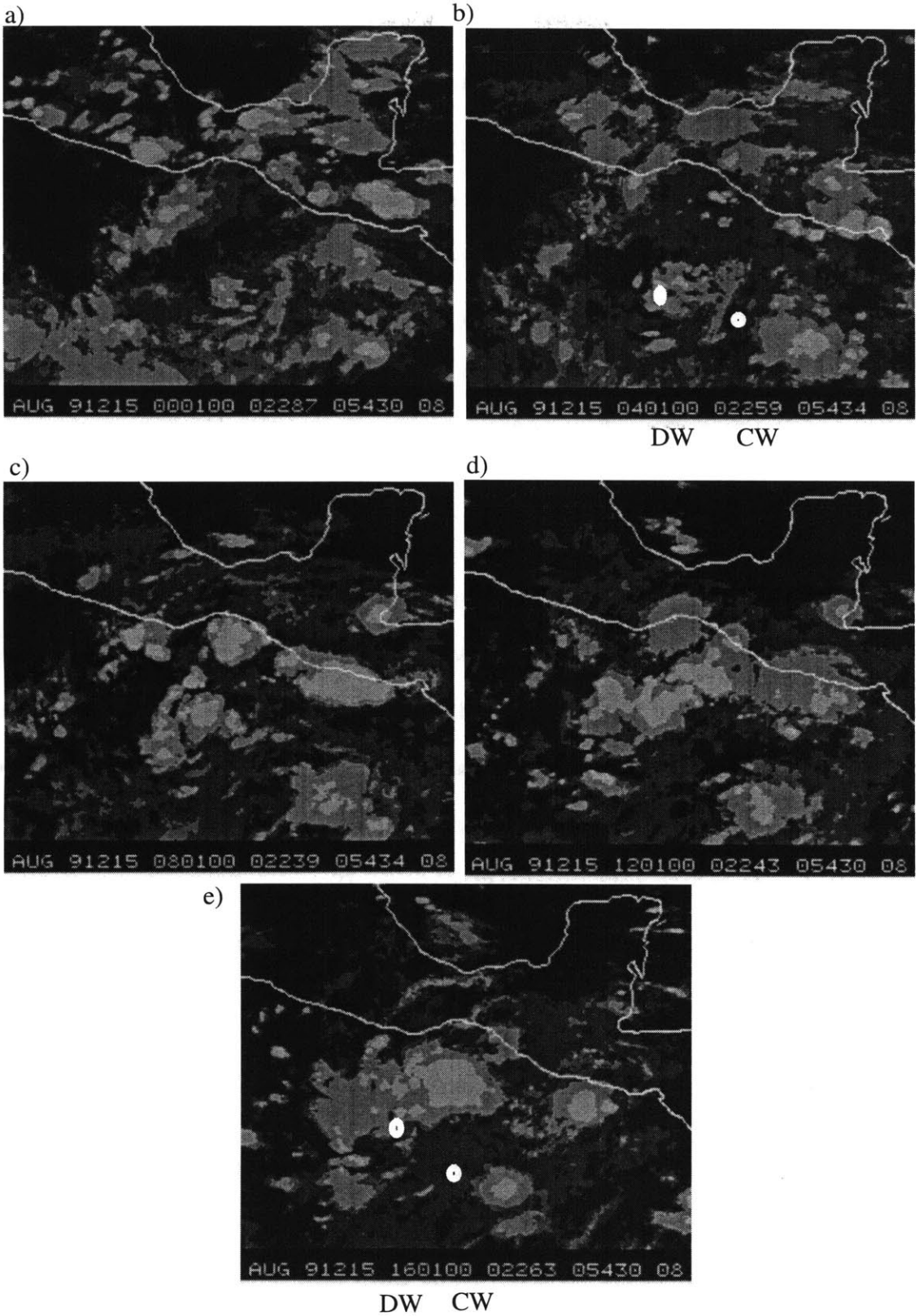


**Figure 3.2:** Same as in Fig. 3.1, but at (a) 00, (b) 04, (c) 08, (d) 12, and (e) 16 UTC on 3 August. The estimated locations of the vortex are shown in similar fashion as in Fig. 3.1

reintensifies (Figs. 3.2 b, c, and d). The few hours after the formation of the MCS is the only time when satellite imagery suggests a linear organization of the system.

In Figures 3.1c, 3.2b, and 3.2e estimates of the location of the vortex are shown. Estimates are obtained from two sources. FZ estimated the location of the vortex from the cloud track wind field at 14 UTC on 2 August and 14 UTC on 3 August, using visible satellite images. I obtained the locations of the center at 04 UTC on 3 August and 07 UTC on 4 August, using an objective analysis of vorticity of the Doppler wind field. In Figures 3.1c and 3.2e the location of the vortex using Doppler wind field has been obtained by extrapolation and interpolation of the data, respectively. In Fig. 3.2b the estimate of the location of the vortex using the cloud track wind field has been obtained by interpolation. It would seem that there are two centers about 200 km apart from each other. However, the estimate of the center using cloud track wind field is more uncertain than the estimate using Doppler wind field. For example, at 14 UTC on August 2 the center using the cloud track wind field should be within 90.0 W and 92 W, and 91.0 W was chosen as the most likely location (L. Farfan, personal communication, 1996).

Note that the vortex center estimated using the Doppler wind field is always in the region of the convection associated with the MCS. However, convection is typically stronger to the north of the vortex than to the south.

### 3.1.2. Vertical shear and midtropospheric humidity

The ECMWF wind analysis at 00 UTC on 3 August 1991 is shown in Figure 3.3. An easterly wave can be seen near Cuba. The region where the vortex was observed during flight 2P at 04 UTC on 3 August is characterized by small vertical wind shear below 500 hPa. There may have been shear associated with the line of convection that is the first

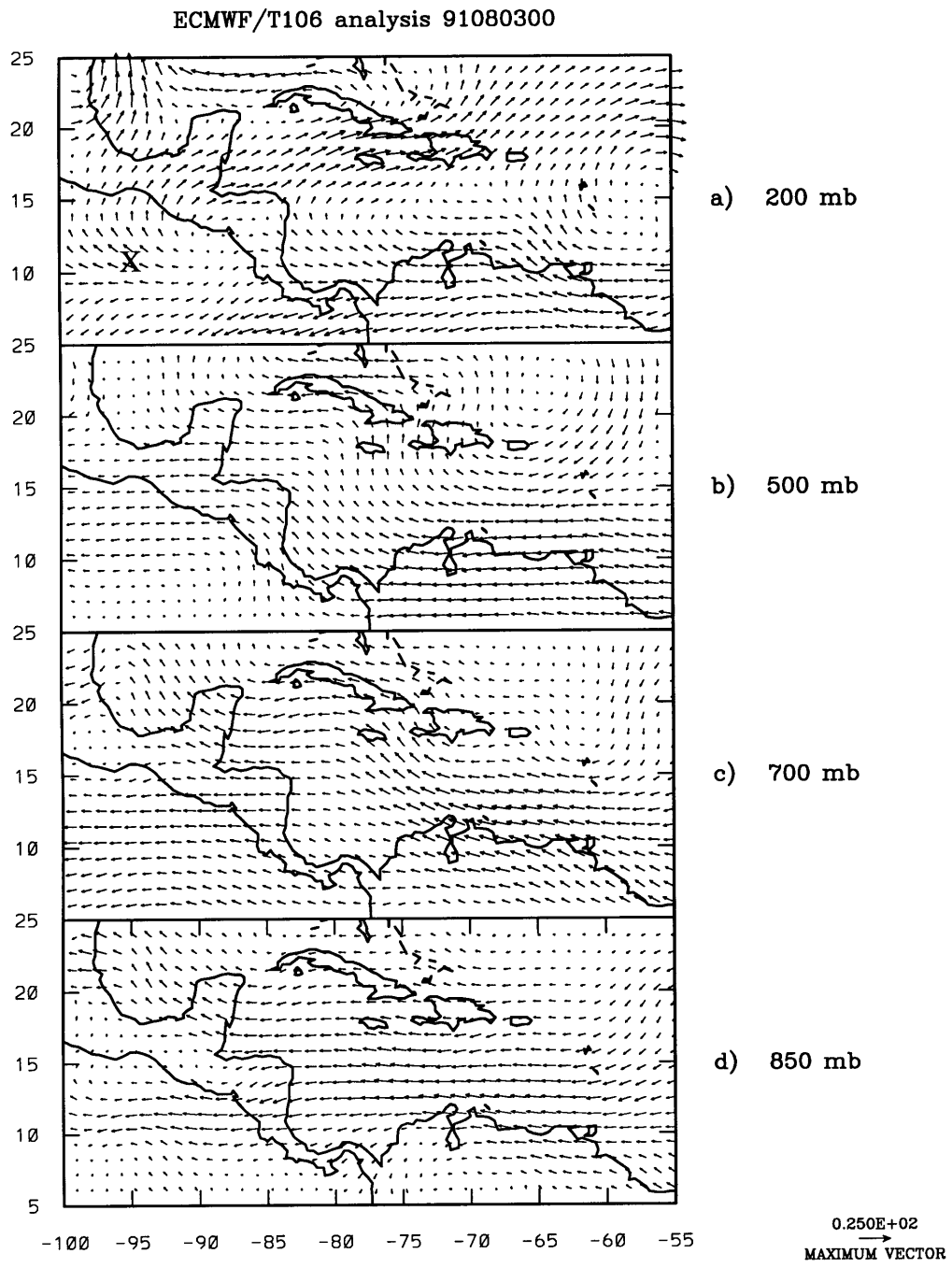


**Figure 3.3:** ECMWF wind analysis at 00 UTC on 3 August, 1991. Location of the vortex is shown in the 200 hPa analysis at 04 UTC on 3 August (cross).

stage of the mesoscale system. However, the rapid disintegration of this line suggests that any shear associated with it has been short-lived. Therefore, we have little reason to believe that horizontal vorticity played a dominant role in the intensification of the vortex.

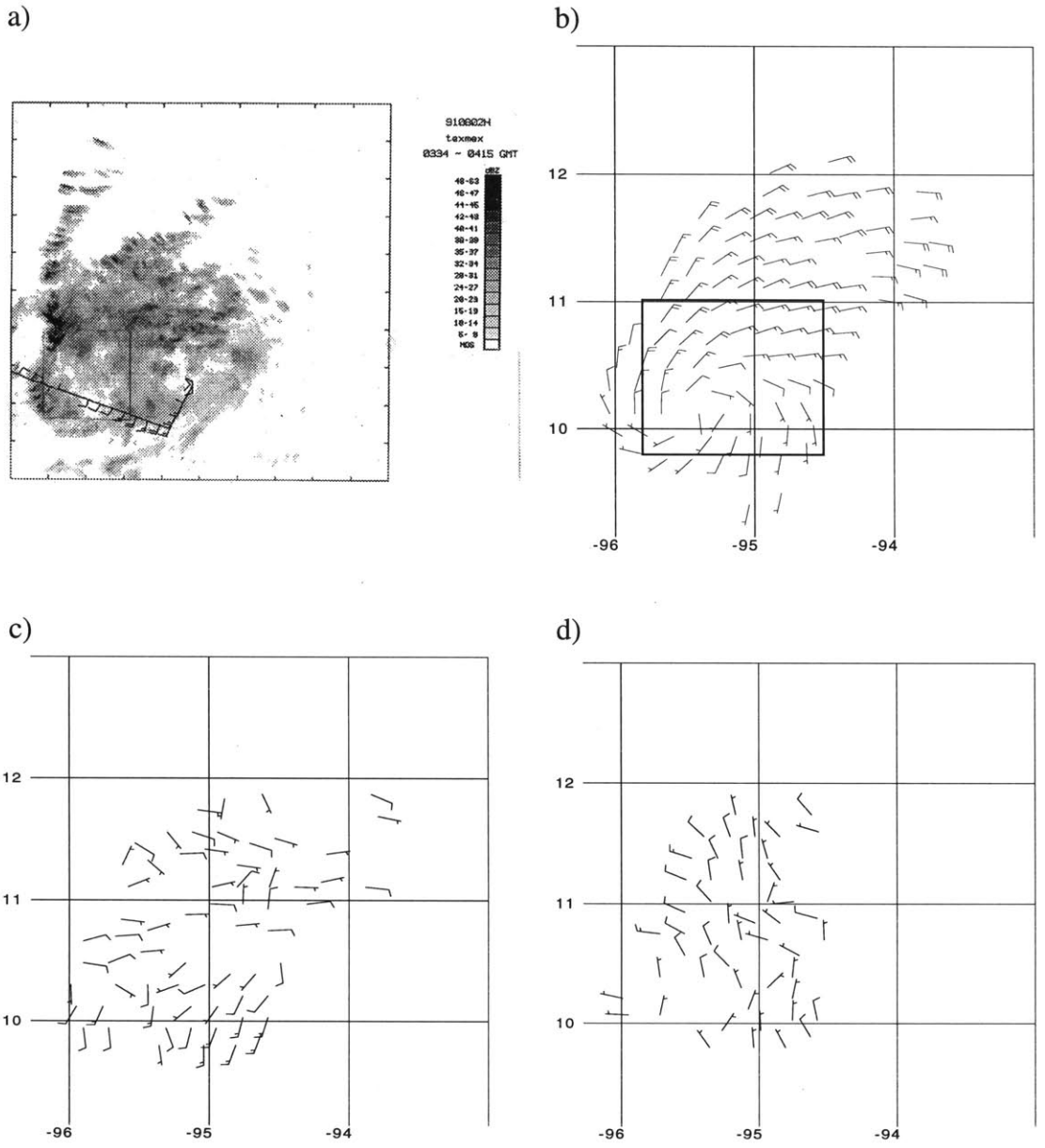


**Figure 3.4:** Radar observations in pre-Guillermo MCS during flight 2P. (a) Radar reflectivity composite from C-band radar, tick marks: 48 km (b) Doppler wind field at 2 km, (c) change of wind from 1 to 3 km, (d) change of wind from 5 to 7 km. Only values larger than 3 $ms^{-1}$ plotted in (c) and (d). Radar data were collected while the aircraft was flying at 3 km altitude. The box in (a) is 10-11 N and 95-96 W. Long barb is 5 $ms^{-1}$.

Both flights 1E and 2P found regions around the mesoscale system where $\Theta_e$ was about 330 K and the relative humidity was about 50% at 700 hPa, showing that the middle troposphere in the environment of the MCS was rather dry.

## 3.2 Flight 2P

The first flight, 1E, was conducted well to the west of the vortex, and on the westernmost part of the MCS. Flight 2P was the first flight into the MCS. In Fig. 3.4, reflectivity measured with the C-band radar and wind measured with the Doppler radar are shown. Figures 3.4a and b show that the mesoscale vortex is in the stratiform region of the precipitation. There is a bright band in the radar reflectivity (not shown) except to the west and north of the vortex, where the values of radar reflectivity are large. Assuming that the vortex is in balance with the thermal field, the change of wind in vertical direction can be used as a proxy for the thermal anomalies in the corresponding layer. The thermal wind relation for flow in hydrostatic and gradient wind balance (e.g. Emanuel 1989) is

$$\frac{1}{r^3}\left(\frac{\partial M^2}{\partial p}\right)_r = \frac{-R}{p}\left(\frac{\partial T_v}{\partial r}\right)_p \tag{3.1}$$

where $M = (0.5 f r^2 + v r)$ is the angular momentum, f is the Coriolis parameter, r is radius, p is pressure, $T_v$ is virtual temperature, v is tangential velocity, and R is the gas constant for air. If the vertical wind shear is anticyclonic (cyclonic), the vortex has a warm (cold) core. The vertical difference between the wind at 3 km and 1 km (Fig. 3.4c), with southwesterly wind difference on the southern side of the vortex and easterly wind difference on the northern side of the vortex, suggests that the vortex is associated with a cold

core in the lower troposphere. The vertical difference between the wind at 7 and 5 km (Fig. 3.4d) suggests a warm core in the upper troposphere, associated with the vortex.

In situ observations from 3 km altitude are shown in Figure 3.5. Relative humidity is about 90% in the region of the vortex. The analysis of virtual potential temperature confirms the existence of a cold core associated with the vortex in the lower troposphere. $\Theta_e$ is relatively uniform with a maximum value of 339 K collocated with the cold and humid core in the center of the vortex. Note that the values of $\Theta_e$ are about 8 K higher than the values found in the environment of the MCS during flights 1E and 2P, and the values of relative humidity are remarkably higher than the value of 50% found in the environment during same flights.

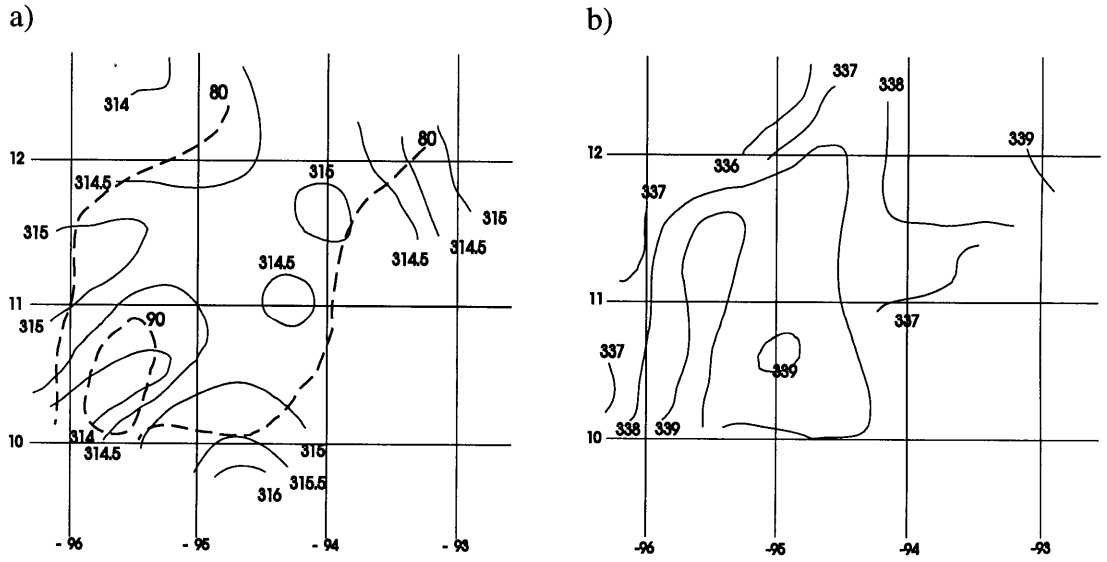


**Figure 3.5:** In situ observations from 3 km altitude in pre-Guillermo MCS during flight 2P. (a) Virtual potential temperature, solid, and relative humidity in percents, dashed; (b) $\Theta_e$. Temperatures in Kelvins.

The analyses of $\Theta_e$ and virtual potential temperature in the boundary layer are shown in Fig. 3.6. In the region of the vortex, both variables have negative anomalies. The negative anomaly of virtual potential temperature in the region of the vortex (see also Fig. 3.4c which implies a negative anomaly in the layer from 1 to 3 km), and the fact that the cold core vortex is found in the stratiform precipitation region suggest that phase changes, especially evaporation and melting of precipitation, could be responsible for the cold core vortex. In principle, adiabatic ascent could also result in a lower tropospheric cold core, with a positive anomaly in relative humidity. However, the fact that the cold anomaly extends to 300 m and is associated with a negative anomaly of $\Theta_e$ at the same altitude is more consistent with a downdraft owing to evaporation of rain and perhaps melting of ice.

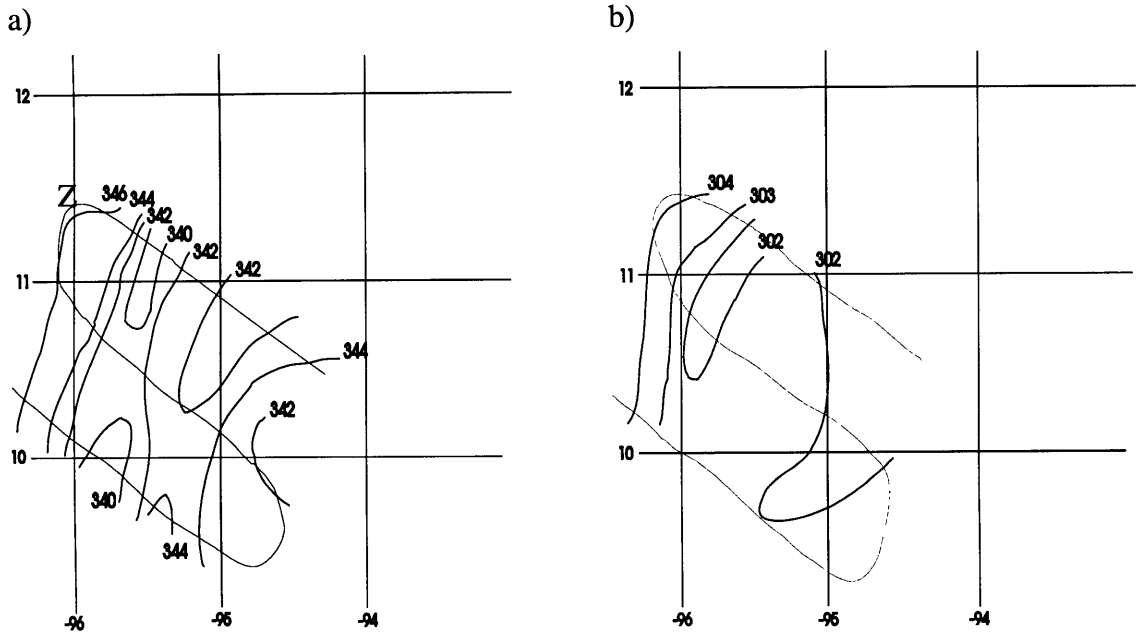


**Figure 3.6:** In situ observations from 300 m altitude in pre-Guillermo MCS during flight 2P. (a) $\Theta_e$,(b) virtual potential temperature. The flight pattern is superimposed in both figures. In (a) letter Z marks location of observation of lightning.

## 3.3 Flight 3E

Owing to the less than optimal flight pattern at 3 km altitude, it is difficult to locate the center of the vortex by looking at the wind field (not shown). However, analysis of the height field of the 700 hPa surface seems to crudely resolve the low pressure center of the vortex. The aircraft flew within a few hectopascals of the 700 hPa level. A correction to 700 hPa was made using the hydrostatic equation and the measured pressure and temperature. The variation of the values of height in Fig. 3.7 corresponds to 2 hPa. The field of virtual potential temperature shows that the low pressure center is associated with a cold core. Values of virtual potential temperature have not changed notably from flight 2P.

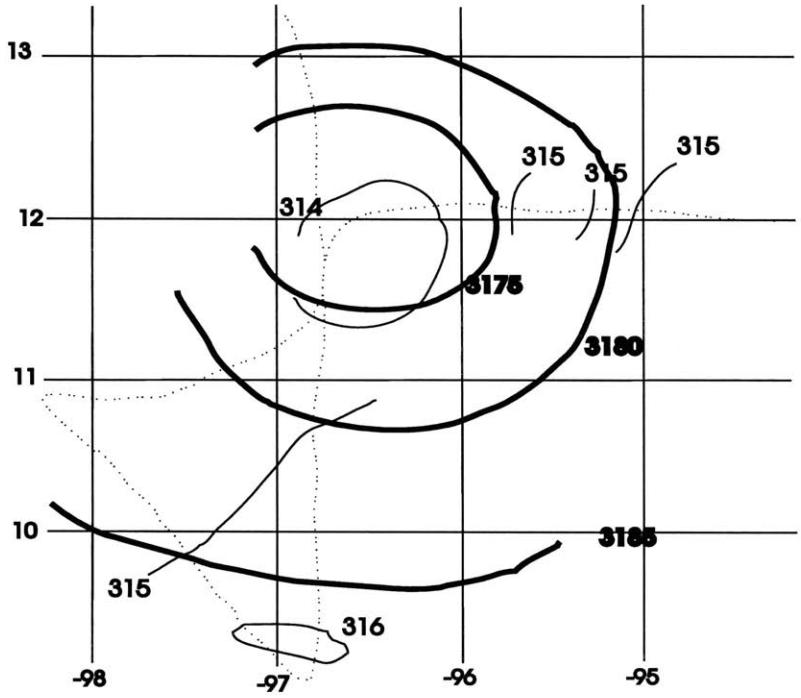


**Figure 3.7:** In situ observations from 3 km altitude in pre-Guillermo MCS during flight 3E. Flight pattern, dots; 700 hPa altitude (m), thick; virtual potential temperature (K), thin

Relative humidity and $\Theta_e$ at 3 km altitude are shown in Figure 3.8. Relative humidity varies mostly between 80 and 90%, with high values near the low pressure center. $\Theta_e$ varies between 334 and 339 K, with high values also near the low pressure center. It seems that the system has changed little at this altitude since flight 2P.

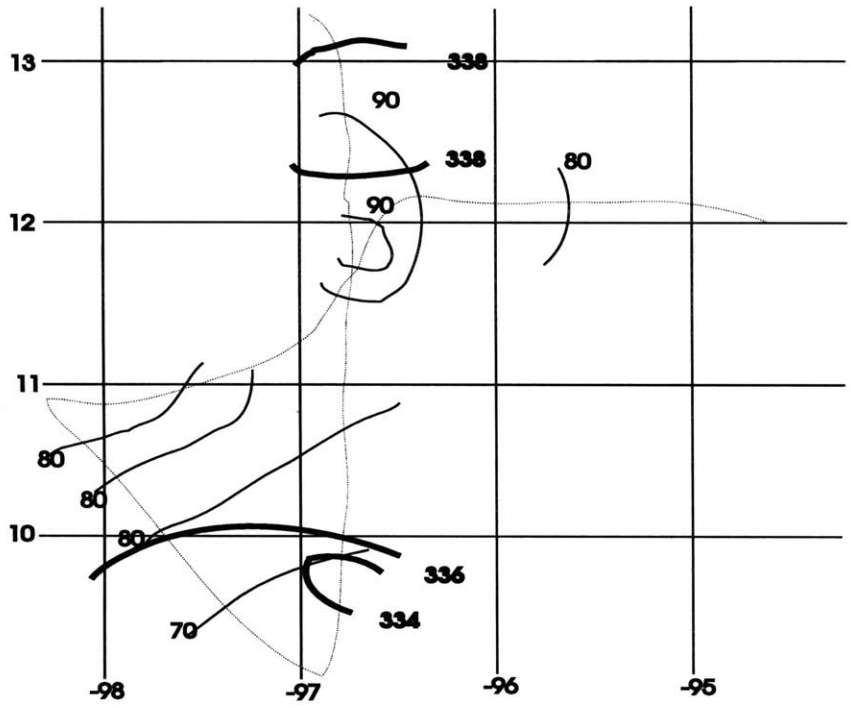


**Figure 3.8:** In situ observations from 3 km altitude in pre-Guillermo MCS during flight 3E. Flight pattern, dots; $\Theta_e$, thick; relative humidity, thin.

The boundary layer flight pattern consists of only one flight leg oriented in an east-west direction at 12.2 N. Relative humidity varies between 78 and 90%. Virtual potential temperature varies between 302 and 304 K, with the smallest values roughly collocated with the low pressure center aloft. $\Theta_e$ varies between 341 and 349 K, with smallest values collocated with the low pressure center as well.

Based on the data from the boundary layer flight leg, it does not seem that there has been notable changes from the previous flight, except that the maximum value of $\Theta_e$ may have increased by a couple of degrees.

## 3.4 Flight 4P

Whereas changes in thermodynamic variables were small between flights 2P and 3E, between flights 3E and 4P a gradual replacement of the lower tropospheric cold core by a warm core inside the cold core had begun. During flight 4P, there is high radar reflectivity mostly on the northern side of the vortex center located at 13.1 N, 99.0 W (Figures 3.9a and b). The change of the Doppler wind between the altitudes of 1.5 and 4.5 km is shown in Fig. 3.9d. The change of wind with altitude is consistent with the analysis of virtual potential temperature at 3 km (Figure 3.10). The vertical wind shear is generally cyclonic, indicating a cold core. But there is a small region with anticyclonic wind shear, displaced slightly north of the center of the vortex, indicating a warm core most clearly on the northern side of the vortex center. Note that the warm core is developing preferentially on the side of the vortex center where convection is strongest. This is also the location where the boundary layer wind speed is largest (not shown). The radar composite from the 300 m flight pattern shows that the intensity of convection has increased, and the location of the most intense convection has moved closer to the center from the time of the 3 km flight pattern (not shown). In Fig. 3.9c Doppler winds are shown at the same altitude as in Fig. 3.9b, but they have been obtained from the boundary layer flight legs. The wind field suggests that vorticity has been concentrated in the center, perhaps owing to convergence to the intensified convection. However, the comparison of in situ wind and Doppler wind, discussed in Chapter 2, shows large inconsistencies between the measurements. The fact that the Doppler wind measurement has additional error sources compared to the in situ

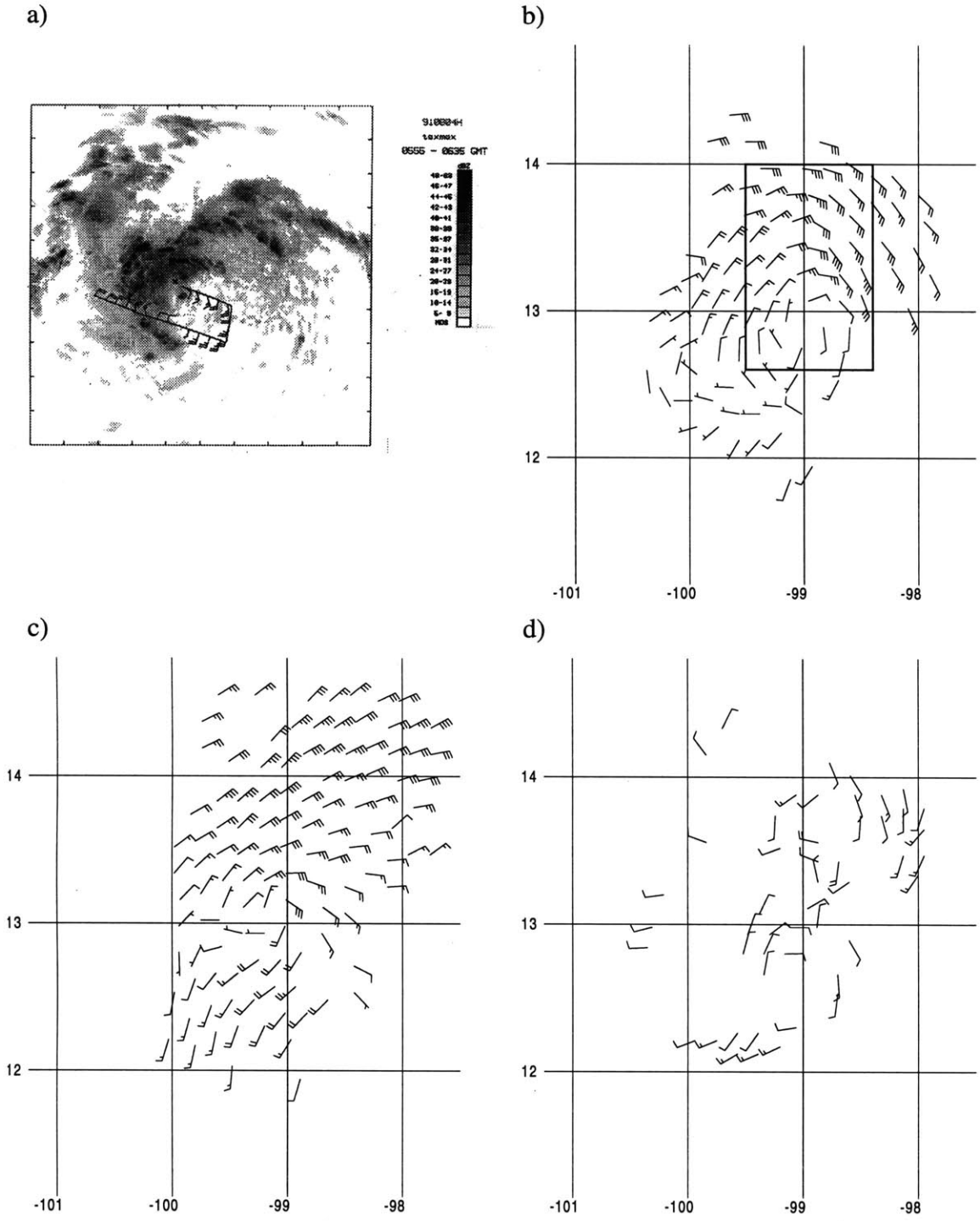


**Figure 3.9:** Radar observations in pre-Guillermo MCS during flight 4P. (a) Radar reflectivity composite, cross marks the center of the vortex, tick marks as in Fig.3.4a, (b) wind at 2 km altitude, (c) wind at 2 km obtained from 300 m flight pattern, (d) change of wind from 1.5 to 4.5 km altitude. Only values larger than 4.5 $ms^{-1}$ are plotted.

wind measurement, and that the in situ measurements show smaller changes in wind field suggest that the differences between the wind fields shown in Figures 3.9b and c may be to a large extent owing to erroneous Doppler winds in Figure 3.9c.

The analysis of virtual potential temperature shows that there is a small warm core inside the cold core both at 3 km and 300 m (Fig. 3.10a). The reversal of the temperature gradient occurs at a larger radius at 700 hPa than in the boundary layer. The analysis of $\Theta_e$ at 700 hPa shows an increase in the values of a couple of degrees from flights 2P and 3E. The values of $\Theta_e$ have also increased in the boundary layer by about 2-3 K in the center of the vortex. The minimum altitude of the 700 hPa surface seems to have decreased by about 15 m between flights 3E and 4P. However, the center was not resolved very well during flight 3E, so the minimum altitude might have been lower than what the analysis suggests.

The analysis of different fields show that the appearance of a small warm core inside the cold core in the lower troposphere is associated with enhanced convection, and increased $\Theta_e$ in the boundary layer. Moreover, the warm core as well as the most intense convection are located slightly to the north of the center of the cold core vortex. This is where the wind speed is largest, and may be associated with increased surface fluxes. On the northern side of the vortex the mean easterly wind would add to the vortex wind, and this may explain the large wind speed there.

## 3.5 Flight 5E

The wind at 3 km altitude during flight 5E is shown in Fig. 3.11a. The system is of tropical storm strength now, with maximum wind exceeding 17 $ms^{-1}$. The warm core at 3 km altitude is now dominant, with the maximum virtual potential temperature 2 K higher than during the previous flight. But there is still a reversal of the gradient of the virtual potential

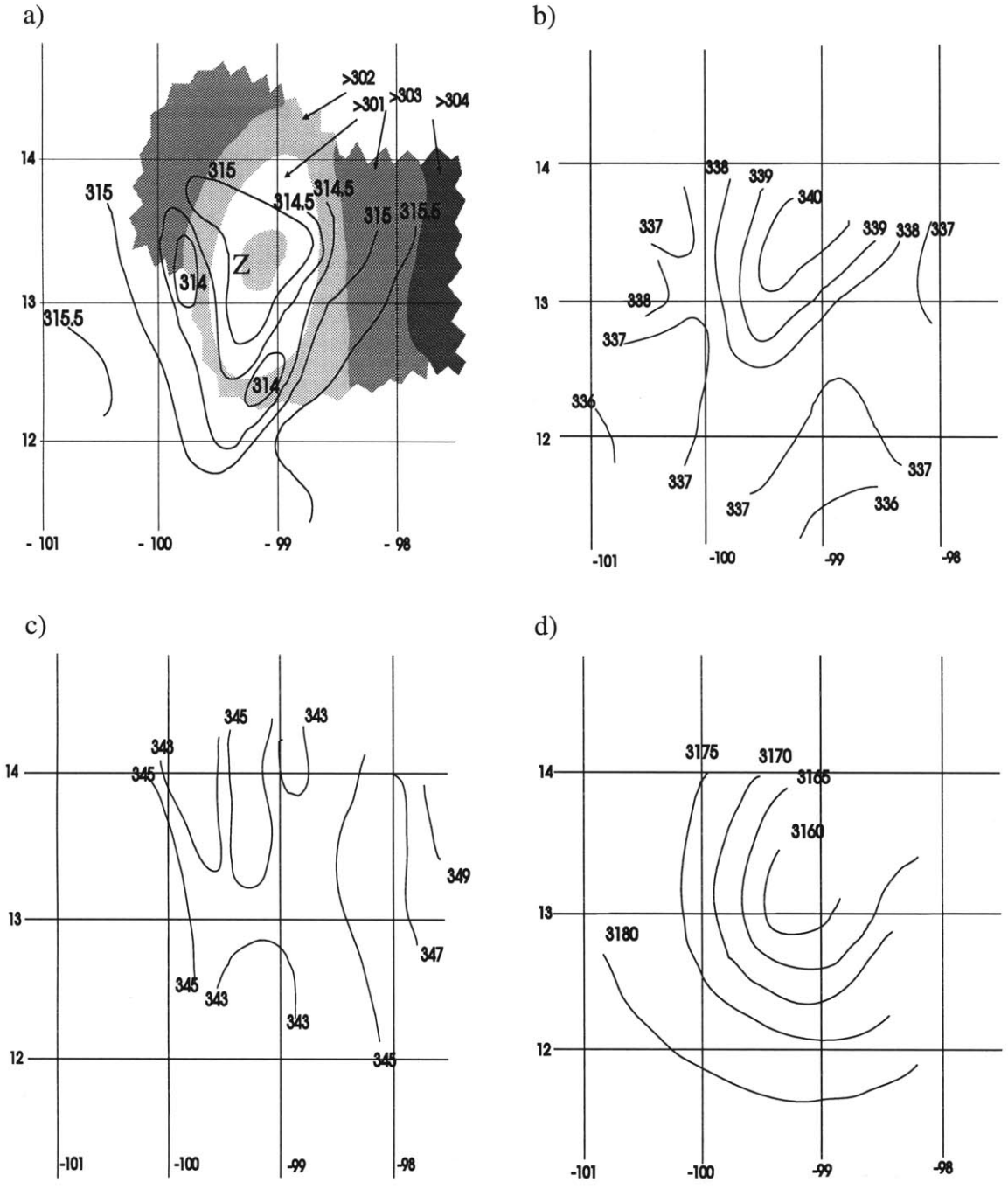


**Figure 3.10:** In situ observations in pre-Guillermo MCS during flight 4P. (a) Virtual potential temperature, 3 km (contours) and 300 m (grey shading); (b) $\Theta_e$, at 3 km; (c) $\Theta_e$, at 300 m; (d) altitude of 700 hPa surface. In (a) letter Z marks location of observation of lightning during the 3 km flight pattern.

temperature about 100 km from the center of the warm core (Fig. 3.11b). The analysis shows it most clearly on the southern side of the storm. The reversal of the temperature gradient is also found in the boundary layer. Even though the maximum values of virtual potential temperature have increased both at 700 hPa and in the boundary layer by about 2 K, the minimum value has not increased.

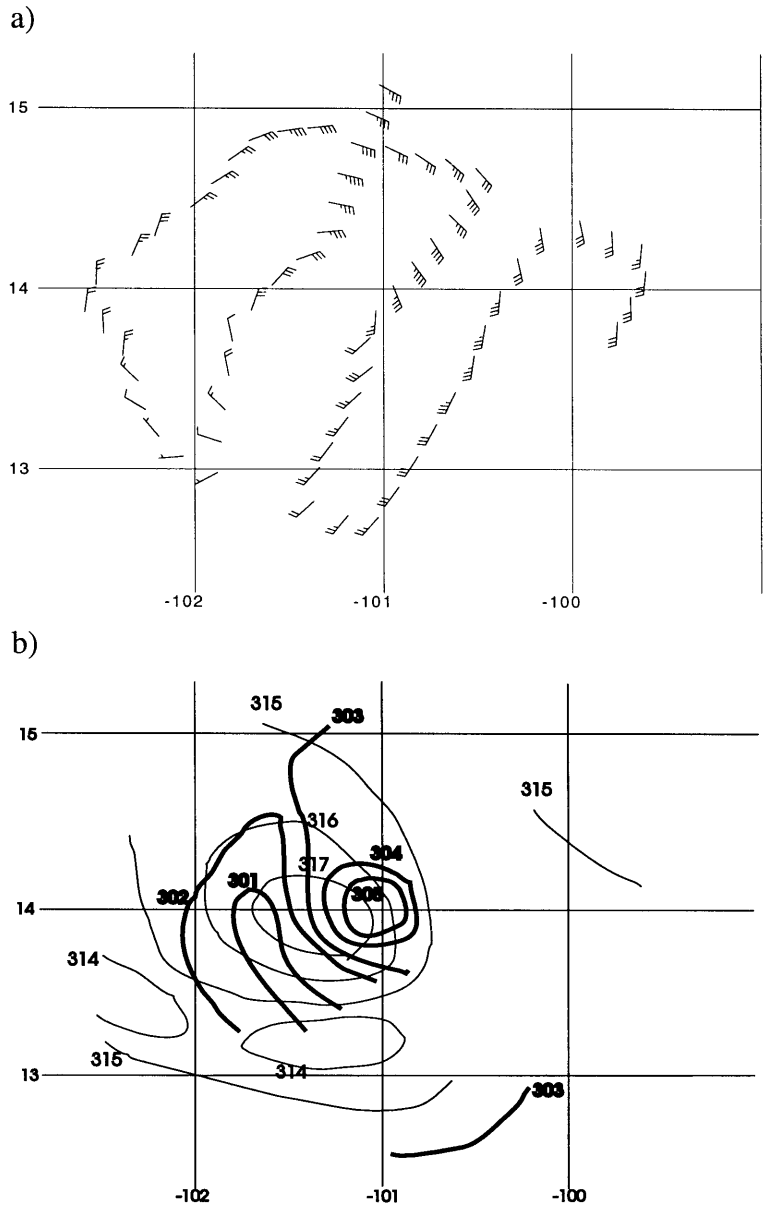


**Figure 3.11:** In situ observations in tropical storm Guillermo during flight 5E. (a) Wind field at 3 km altitude (b) virtual potential temperature at 3 km (thin) and at 300 m (thick).

## 3.6 Flight 6P

During the last flight of IOP 5, tropical storm Guillermo was declared a hurricane by the National Hurricane Center. The maximum wind in the boundary layer (not shown) was about 70 knots (35 $ms^{-1}$). The change of wind with altitude (Fig. 3.12c) shows that the system is associated with a lower tropospheric warm core. In situ analysis shows that the

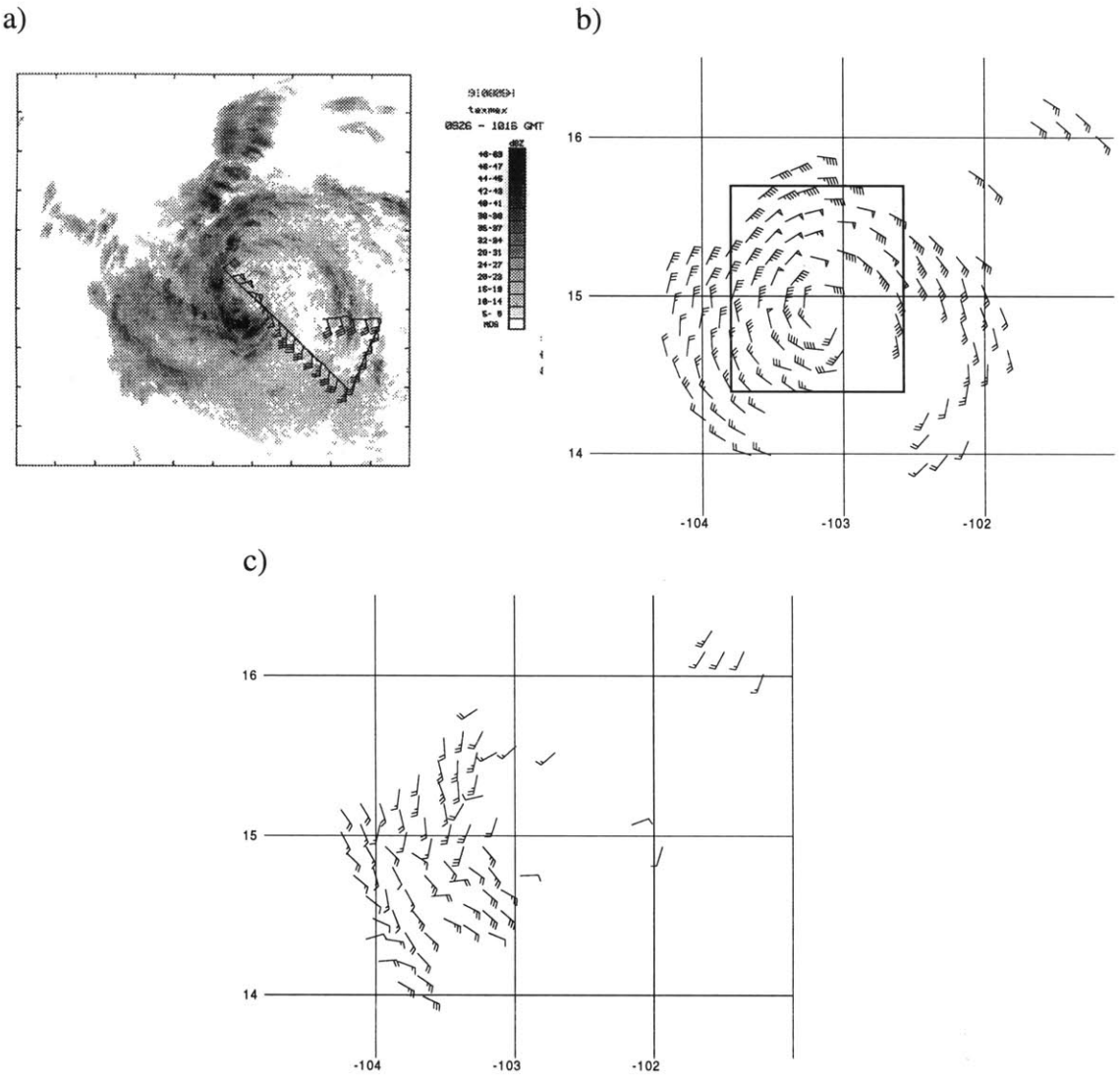


**Figure 3.12:** Radar observations in hurricane Guillermo during flight 6P. (a) Radar reflectivity composite as in Fig. 3.4a, (b) wind field at 2 km altitude, (c) change of wind from 1.5 km to 4.5 km altitude, only values larger than 4.5 $ms^{-1}$ are plotted

minimum pressure at 300 m altitude is 962 hPa (Fig. 3.13a), about 10 hPa lower than 80 km from the center of the hurricane. The maximum virtual potential temperature at 700 hPa is 320 K (Fig. 3.13b), about 5 K higher than what seems to have been the environmental value during the earlier flights.

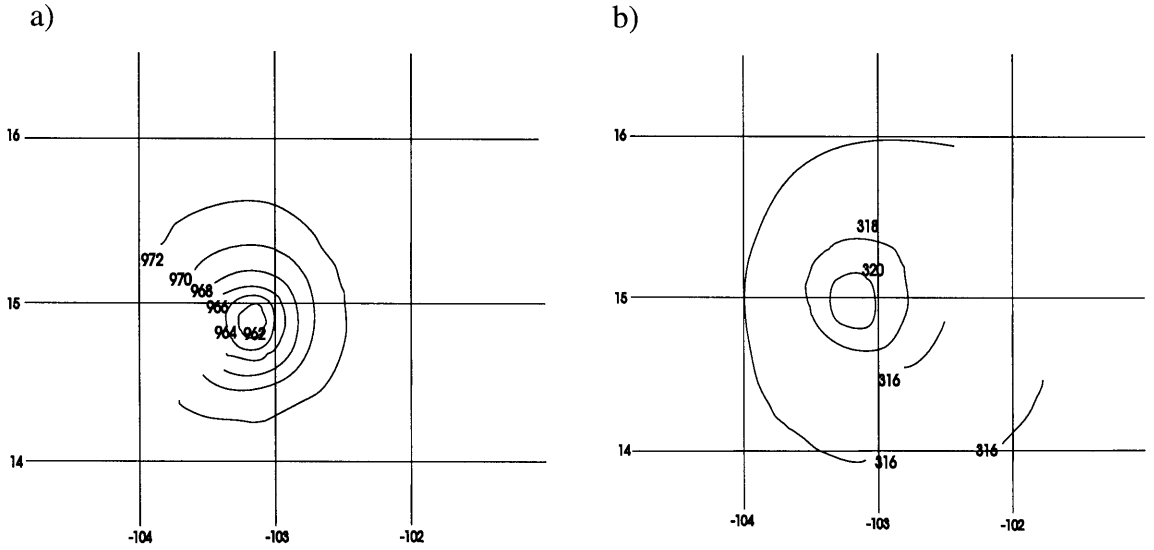


**Figure 3.13:** In situ observations in hurricane Guillermo during flight 6P. (a) Pressure at 300 m, (b) virtual potential temperature at 3 km.

To get a rough estimate of the changes of thermodynamic variables in the region of the vortex, averages were calculated in a box of roughly 140 km in the zonal and meridional directions. The box was chosen to be centered on the vortex. The center was estimated using analysed vorticities from Doppler winds. Since Doppler winds are available only from flights 2P, 4P, and 6P, averages were calculated only for these three flights. In one case the vorticity analysis showed that the vorticity was elongated in the north-south direction. The box was then chosen to be slightly elongated in the same direction. The

boxes for which the averages were calculated are shown in Figures 3.4b, 3.9b, and 3.12b. No weighting was used in the calculation of the average. Note that the time difference between each pair of consecutive flights is 28 hours. The results are shown in Table 3.1.

| Variable and altitude | Flight 2P | Flight 4P | Flight 6P |
|---|---|---|---|
| RH, 3 km | 83 | 85 | 81 |
| RH, 0.3 km | 85 | 92 | 91 |
| $\Theta_e$, 3 km | 338 | 339 | 345 |
| $\Theta_e$, 0.3 km | 342 | 345 | 350 |
| $\Theta_v$, 3 km | 315 | 315 | 318 |
| $\Theta_v$, 0.3 km | 302 | 302 | 304 |

**Table 3.1: Averages of in situ data in a box around the vortex from the two flight altitudes for flights 2P, 4P, and 6P. Relative humidity in percents, temperature variables in Kelvins.**

Note that there is little change in the relative humidity, $\Theta_e$, and virtual potential temperature at 3 km altitude between flights 2P and 4P. However, in the boundary layer relative humidity increases by 7% and $\Theta_e$ increases by 3 K between these flights. This suggests that between the cold core stage and the development of the small warm core inside the cold core the system's main thermodynamic change is moistening of the boundary layer.

The development to a hurricane, between flights 4P and 6P, is associated with an increase of $\Theta_e$ of about 5 K in both the boundary layer and at 3 km altitude, and an increase of virtual potential temperature of about 2-3 degrees at both altitudes. The increase of $\Theta_e$ and virtual potential temperature in the boundary layer and at 3 km altitude while the tangential wind speed increases suggests that the intensification owing to the feedback of the wind and the surface heat fluxes is in operation.

It is interesting to note that the maximum value of $\Theta_e$ at 3 km can be found in the center of the cold core vortex during flight 2P. This fact suggests that mesoscale downdraft could have increased $\Theta_e$ at 3 km, presumably by importing higher values from aloft.

## 3.7 Conclusion

The observation of the humid cold core vortex in the stratiform precipitation region suggests that evaporation (and possibly melting) might be partially responsible for its formation. A humid cold core could also result from adiabatic ascent. However, the fact that the vortex is associated with a strong negative anomaly of $\Theta_e$ and virtual potential temperature even in the boundary layer and that the negative anomaly of virtual potential temperature is also found between 1 and 3 km during flight 2P (Fig. 3.4c) suggests that it be owing to phase changes and not due to adiabatic ascent.

A simple numerical experiment was designed to study the formation of a vortex with a lower tropospheric humid cold core. **The goal of the experiment is to test the hypothesis that cooling by evaporation of mesoscale stratiform rain can lead to a humid cold core vortex that can initiate tropical cyclogenesis.** The absence of vertical shear and the nonlinear character of the MCS justify the use of an axisymmetric model, which will be described in the following section. A second set of experiments will be carried out to study whether the cold core vortex or the increased midtropospheric humidity is more important for cyclogenesis in the model.

Possible heating in the anvil, from which the stratiform precipitation supposedly falls, will not be considered in the model. Heating in the upper troposphere would mostly be associated with convergence in the midtroposphere and vertical advection of vorticity upward, whereas the advection of vorticity associated with evaporational cooling is downward. And low level winds should be more important for cyclogenesis, because of their

role in surface heat fluxes and inertial stability in the lower troposphere. Another reason for not accounting for heating in the anvil will be discussed in Chapter 5.

# Chapter 4

# Numerical model

The model used in this study was developed by RE. It has many similarities with the cloud model developed by Klemp and Wilhelmson (1978, KW hereinafter), including the use of fully compressible, nonhydrostatic equations of motion with a splitting procedure that treats sound waves separately, and open lateral boundary conditions that permit gravity waves to propagate out of the integration domain. The models differ in subgrid-scale parameterizations. Furthermore, the KW model is three-dimensional, whereas the RE model is two-dimensional and axisymmetric. Two-dimensionality is a necessary restriction owing to the largeness of the domain needed to simulate a hurricane.

The original RE model had only one liquid water variable. Therefore no difference was allowed in the evaporation rates or terminal velocities of cloud and rain water. I incorporated predictive equations for cloud and rain water mixing ratios, and employed Kessler-type microphysics. This change was crucial since evaporation of precipitation has the key role in the hypothesis to be tested with the model. The physics of the model is discussed in section 4.1. The changes made to the microphysics are discussed in section 4.2, and the numerics are discussed in section 4.3.

## 4.1 Physics of the model

The model equations describe fully compressible, nonhydrostatic motions in an axisymmetric framework. Cylindrical coordinates $(r,\phi,z)$ are employed. The original seven dependent variables are radial (u), azimuthal (v), and vertical (w) wind velocities; nondimensional pressure perturbation from the initial state ($\pi$); potential temperature ($\Theta$); mixing ratio of water vapor ($q_v$); and mixing ratio of liquid water ($q_l$). The nondimensional

pressure is defined as

$$\pi = \left(\frac{p}{p_0}\right)^{R_d/c_p} \tag{4.1}$$

where $R_d$ is the gas constant for dry air, and $p_0$ is the base state pressure at the ground.

The predictive equations for the seven dependent variables are:

$$\frac{du}{dt} - \left(f + \frac{v}{r}\right)v = -c_p\overline{\Theta}_v\frac{\partial\pi}{\partial r} + D_u \tag{4.2}$$

$$\frac{dv}{dt} - \left(f + \frac{v}{r}\right)u = D_v \tag{4.3}$$

$$\frac{dw}{dt} = -c_p\overline{\Theta}_v\frac{\partial\pi}{\partial z} + D_w + g\left\{\frac{\Theta - \overline{\Theta}}{\overline{\Theta}} + 0.61\,(q_v - \overline{q_v}) - q_l\right\} \tag{4.4}$$

$$\frac{\partial\pi}{\partial t} + \frac{\bar{c}^2}{c_p\overline{\rho}\overline{\Theta}_v^2}\left\{\frac{1}{r}\frac{\partial}{\partial r}(ru\overline{\rho}\overline{\Theta}_v) + \frac{\partial}{\partial z}(w\overline{\rho}\overline{\Theta}_v)\right\} = 0 \tag{4.5}$$

$$\frac{d\Theta}{dt} = M_\Theta + D_\Theta \tag{4.6}$$

$$\frac{dq_v}{dt} = M_{q_v} + D_{q_v} \tag{4.7}$$

$$\frac{dq_l}{dt} = M_{q_l} + D_{q_l} \tag{4.8}$$

In these equations f is the Coriolis parameter, $c_p$ is the specific heat of dry air at constant pressure, $\Theta_v$ is the virtual potential temperature, g is the acceleration due to gravity, c is the speed of sound, and $\rho$ is the density of the mixture of air and vapor. Quantities with an overbar are initial-state variables, and are functions of z only. The symbols M and D denote microphysical and diffusive terms, respectively.

The pressure tendency equation was derived from the mass continuity equation without assuming anelasticity. The equations are therefore capable of representing sound waves. Owing to the fast propagation speed of the sound waves and the CFL criterion, the equations must be integrated with a time step small enough for the propagation of the sound waves not to be aliased. RE follow KW in computing only those terms associated with sound waves with a small time step, and the rest are computed with a time step determined from the advective and diffusive processes. For more information about this separation see KW.

Turbulence is formulated following the treatment of Mason and Sykes (1982). The diffusional terms are formally derived by azimuthally averaging the equations in cylindrical coordinates, and dividing the dependent variables into an azimuthal average and a departure from it. The terms containing the departure terms are Reynold's stresses and fluxes owing to azimuthal variations on the azimuthally averaged flow. To get the stresses and fluxes as a function of the azimuthally averaged flow, the eddy-viscosity assumption is made. RE follow Lilly (1962) in forming an energy equation for turbulence, and assuming equilibrium conditions for turbulent energy. The vertical flux of buoyancy, in the equation for turbulent energy, depends on whether air is saturated or not, and dissipation of turbulent energy depends on the eddy viscosity and the length scale of eddies, on dimensional grounds. The energy equation is solved for the eddy viscosity. The length scale of the eddies is specified as a function of the grid size. The fact that the vertical grid size is

smaller than the horizontal grid size is accounted for by defining a separate horizontal viscosity based on the horizontal grid size (see Table 4.1).

## 4.2 New microphysics scheme

RE used only one class of liquid water. Here, predictive equations are formulated for both cloud and rain mixing ratios using a Kessler-type parameterization. The equations for the cloud and rain water mixing ratios are

$$\frac{dq_c}{dt} = M_{q_c} + D_{q_c} \tag{4.9}$$

$$\frac{dq_r}{dt} = M_{q_r} + D_{q_r}. \tag{4.10}$$

The microphysical terms are

$$M_\Theta = -\gamma\left(\frac{dq_{vs}}{dt} + E_r\right) \tag{4.11}$$

$$M_{q_v} = \frac{dq_{vs}}{dt} + E_r \tag{4.12}$$

$$M_{q_c} = -\frac{dq_{vs}}{dt} - A_r - C_r \tag{4.13}$$

$$M_{q_r} = \frac{1}{\bar{\rho}}\frac{\partial}{\partial z}(\bar{\rho} V_t q_r) - E_r + A_r + C_r . \tag{4.14}$$

$A_r$, and $C_r$, represent the autoconversion and accretion of cloud particles, respectively. $E_r$ represents evaporation of rain. In equation (4.11) $\gamma = L / (c_p \pi)$, where $\pi$ is the total nondimensional pressure, and L is the latent heat of vaporization. $q_{vs}$ is the saturation mixing ratio, and $dq_{vs}/dt$ is the condensation or evaporation of cloud water. $V_t$ is the terminal velocity of rainwater (equation 4.22). The microphysical terms are same as those in KW, except for the evaporation rate of rain water and terminal velocity. The conversion between water vapor and cloud water is originally from Soong and Ogura (1973). The autoconversion and accretion rates are

$$A_r = k_1 (q_c - a) \tag{4.15}$$

$$C_r = k_2 q_c q_r^{0.875} . \tag{4.16}$$

Here $k_1 = 0.001\ s^{-1}$, $a = 0.001$, and $k_2 = 2.2\ s^{-1}$.

Evaporation of rain, $E_r$ was derived in the following way. The diffusional growth equation for a drop is (Rogers and Yau 1989)

$$\frac{dm}{dt} = \frac{4\pi r (S-1)}{a+b}, \tag{4.17}$$

where a is a coefficient associated with heat conduction and b is a coefficient associated with vapor diffusion. Both terms depend weakly on temperature. If a droplet moves with respect to the surrounding air, ventilation has to be accounted for. The ventilation factor was taken from Ogura and Takahashi (1971)

$$C = 1.6 + 0.57\times10^{-3} V_t^{1.5}, \tag{4.18}$$

where $V_t$ is the terminal velocity, and is given by

$$V_t = V_0 D^{0.5}. \tag{4.19}$$

Here $V_0$ is 13 $ms^{-1}$ and D is the diameter of the drop in centimeters. This formula comes originally from Kessler (1969).

To get the evaporation as a function of rain mixing ratio, an assumption has to be made about the drop size distribution. The drop size distribution was assumed to obey the Marshall-Palmer (MP hereinafter) logarithmic distribution (see e.g. Rogers and Yau 1989)

$$N(D) = N_0 e^{-\lambda D}, \tag{4.20}$$

where *N(D)dD* is the number of drops per unit volume with diameters between *D* and *D+dD*, and $N_0 = 0.08$ $cm^{-4}$. The evaporation rate is obtained by integrating the diffusional growth equation over all drop sizes. The evaporation rate becomes

$$E_r = \frac{1}{\bar{\rho}} \frac{(1-S)}{a+b} \sqrt{\frac{4\pi n_0}{\rho_w}} \sqrt{\bar{\rho} q_r} \left( 1.6 + 55.7 \left(\bar{\rho} q_r\right)^{0.1875} \right). \tag{4.21}$$

Here S is the saturation ratio $q_v/q_{vs}$, and evaporation only occurs if S is less than 1. $\rho_w$ is the density of liquid water.To get values for constants a and b, 283 K was used for temperature. The evaporation rate of equation (4.21) differs from the evaporation rate used by KW, which originally comes from Ogura and Takahashi (1971). The different dependence on the rain mixing ratio is partly owing to the fact that in my derivation the expression for the ventilation factor was used in the integration of drop sizes, whereas Ogura and Taka-

hashi seem to have treated the ventilation factor as a constant in the integration.

The representative terminal velocity was calculated using equation (4.19), and assuming an MP drop size distribution,

$$V_t = 29.94\,(\bar{\rho} q_r)^{0.125}\left(\frac{\bar{\rho}}{\rho_0}\right)^{-0.5}, \tag{4.22}$$

where $\rho_0$ is the basic state density at the ground. The density factor that accounts for mean density variations, was originally suggested by Kessler (1969).

Note that the drop size distribution was assumed to obey the Marshall-Palmer logarithmic size distribution. However, in the presence of evaporation, small drops are evaporated faster than larger drops. This tends to drive the size distribution away from an MP size distribution. Since I suspected that the amount of precipitation reaching lower altitudes might be important for extending cooling over a larger vertical distance, I checked whether getting rid of the MP size distribution assumption would lead to more rain water at lower altitudes. I made the assumption that only evaporation can change the mixing ratio of rainwater. It is then possible to calculate the drop size distribution as a function of mixing ratio, and use the distribution to calculate the terminal velocity and amount of evaporation in the model. Indeed the results showed that there was more rainwater reaching the boundary layer. However, the relative amount of evaporation at low altitudes was not larger than when the MP size distribution was used, apparently owing to the large radius of drops that reach these low altitudes.

## 4.3 Numerics

In this section the boundary conditions, numerical integration and derivation, and numerical parameters are discussed. The open lateral boundary condition is same as in KW. The

purpose is to let gravity waves leave the domain of integration with as little reflection at the lateral boundary as possible. In case of outflow (positive u), the radial momentum equation is replaced by

$$\frac{\partial u}{\partial t} + (u + c_{int})\frac{\partial u}{\partial r} = \left(f + \frac{v}{r}\right)v, \tag{4.23}$$

where $c_{int}$ is the intrinsic phase velocity of the dominant gravity wave mode. All the other variables are calculated using the model equations with one-sided differences for required normal derivatives. In the case of inflow, the normal advection terms are set to zero in the other prognostic equations. If $(u + c_{int})$ is negative, the advection term is set to zero also in equation (4.23). KW present an analysis of reflection of a periodic gravity wave at the open boundary with two-dimensional linear equations. The reflection is eliminated if $c_{int}$ is equal to the phase speed of the gravity wave. Less reflection is caused if $c_{int}$ is overestimated than if it is underestimated. Based on this result, KW choose $c_{int}$ to correspond to the phase speed of the faster propagating modes, with a value of 30 $ms^{-1}$.

At the lower and upper boundary w is required to vanish. To damp gravity waves before they reflect from the rigid lid back to the lower troposphere, a sponge layer is employed in the uppermost portion of the model, well above the tropopause. In the sponge layer, Newtonian damping is added to the right hand side of all prognostic equations, except for the equation for $\pi$.

At the lower boundary the tangential stresses and vertical fluxes are given by the bulk aerodynamic formulas:

$$\left[C_D u (u^2 + v^2)^{1/2}\right]_{(\Delta z)/2} \tag{4.24}$$

$$\left[C_D v\,(u^2+v^2)^{1/2}\right]_{(\Delta z)/2} \tag{4.25}$$

$$\left[C_E (u^2+v^2)^{1/2}\right]_{(\Delta z)/2} (\Theta_{surf} - \Theta|_{(\Delta z)/2}) \tag{4.26}$$

$$\left[C_E (u^2+v^2)^{1/2}\right]_{(\Delta z)/2} (q_{v_{surf}} - q_v|_{(\Delta z)/2}) \,. \tag{4.27}$$

Here $C_D$ and $C_E$ are drag coefficients for momentum and (sensible and latent) heat that are assumed to be equal, and $\Delta z$ is the vertical resolution. The drag coefficients are given by (see Moss and Rosenthal, 1975)

$$C_{D,E} = 1.1\times10^{-3} + 4\times10^{-5}\,(u^2+v^2)^{0.5}\big|_{(\Delta z)/2} \,. \tag{4.28}$$

A spatially staggered grid is used, where the grid points for u and w are displaced by one-half grid point in the x and z directions, respectively, from the grid point where all other variables are defined. This results in improved resolution for certain important terms. Standard second-order differences are used for spatial derivatives. However, for the fall of precipitation, upstream differencing is used. Leap-frog scheme is used for time-integration, except for the integration of the sound wave portion (see KW for details). Since the computational mode of the leap-frog scheme is unstable for frictional terms, forward integration is used for frictional terms. To avoid the tendency of splitting of solutions of the Leap-frog scheme, the weak Asselin time-filter of KW is used.

The original model parameters and the model parameters to be used in simulations that are discussed in Chapter 5 and 6 (except where otherwise noted) are given in Table 4.1. The domain top and the bottom of the sponge layer were moved 5 km upward, because

with the old values there were sometimes vertical velocities of a couple meters per second even in the sponge layer. The temperature structure between 25 and 30 km was taken from the climatological values of Newell et al. (1972) for June -August, at latitude 10 N, as shown in Lindzen (1990). This change, however, affected the results of the integration little.

| Parameter | Description | RE value | New value |
|---|---|---|---|
| $l_0$ | Mixing length | 200 m | same as old |
| $l_H$ | Horizontal mixing length | 3000 m | 1500 m |
| $z_{sponge}$ | Bottom of sponge layer | 19.375 km | 24.375 km |
| $z_{top}$ | Domain top | 25 km | 30 km |
| $r_{outer}$ | Domain outer radius | 1500 km | 3000 km |
| $\Delta z$ | Vertical grid size | 1.25 km | same as old |
| $\Delta r$ | Horizontal grid size | 15 km | 7.5 km |
| $\Delta t$ | Time step | 20 s | 10 s |
| f | Coriolis parameter | $5 \times 10^{-5}$ $s^{-1}$ | $3 \times 10^{-5}$ $s^{-1}$ |

**Table 4.1: Model parameters used in RE and in present simulations**

Initially, a horizontal resolution of 15 km was used in the simulations. However, when a smaller resolution of 7.5 km was used, the results were different. It is likely that the very small scale of the storm in the present simulations could not be simulated with 15 km resolution. The storm that forms in the control simulation, to be discussed in Chapter 5, has a radius of maximum winds at about 20 km from the center. Owing to an increase in the spatial resolution, the time step also needed to be reduced.

The domain outer radius was increased from 1500 km to 3000 km, since the results were different for these two values. The outer radius of 3000 km seemed to be enough, since increasing the outer radius further to 6000 km did not change the results. The need to use the higher outer radius might be owing to several things. First, due to the initial state of no motion, the Rossby radius of deformation is very large. Therefore gravity waves, originated in the center of the domain, can propagate over larger distances. Second, in the course of the simulation, the vertical scale, and thus also the phase speed of the dominant gravity waves, change remarkably, unlike in the simulations of RE. Therefore, using only one value for $c_{int}$ might result in the dominant waves being reflected some time in the course of the integration. Third, RE used Newtonian cooling in their simulations. In the present simulations no radiational cooling is used. This probably also results in gravity waves propagating over larger distances. By increasing the domain outer radius, the hydrostatic gravity waves have more time to be affected by rotation or dissipation, and are less likely to be reflected from the outer wall.

Increasing the vertical resolution to 625 m did not affect the simulation. Therefore, the original resolution of 1250 m was kept.

# Chapter 5

# Rainshower simulations

The data analysis shown in Chapter 3 suggests that evaporation of precipitation and perhaps melting could at least partially account for the cold core vortex. The reason why diabatic heating in the upper troposphere may not be of first order importance is that it is not associated with a vortex in the **lower troposphere**, and it would presumably be associated with increase of relative humidity at those altitudes only, where the adiabatic ascent prevails. However, there is another reason for not considering condensation in clouds. This has to do with the fact that convection in quasi-equilibrium with forcing is a response to the forcing, e.g. destabilization associated with radiative cooling or large-scale ascent. Indeed, Cotton and Anthes (1989, p. 594) note that there is a tendency for MCSs to develop in regions of large-scale ascent. So it is probable that the deep convective heating is partially or completely canceled by the forcing. As the matter of fact, Emanuel et al. (1994) claim that large-scale systems in the tropics feel a small positive effective stability, therefore large-scale ascent results in **cooling**. In case of condensation, one would not only need to account for the heating, but also for the destabilization that causes convection. Therefore, it would be rather artificial to implement in the model some form of condensation without accounting for the forcing.

Unlike condensation, evaporation of rain is not a direct response to a forcing. If evaporation of rain cannot lead to tropical cyclogenesis, it may be that condensation in the MCS indeed is important. We would then need to study a system with realistic forcing for convection. This means that we would need to be able to simulate (and understand!) the formation of MCSs.

Radiation will not be accounted for in the simulations. Radiation can be of importance to the precipitation fields in MCSs due to domainwise destabilization and differential stabilization in vertical or horizontal direction. Even though radiational effects can increase precipitation in MCSs, consistency demands that we neglect radiation since we also neglect condensation in clouds. However, it should be noted that for a mature hurricane radiation is important as a heat sink, and prevents the outer regions from warming up.

It has been shown by Fjørtoft (1953) and discussed by Kundu (1990) that turbulence in two dimensions causes upscale energy cascade. The reason, as explained by Kundu, is the absence of vortex stretching in two dimensions. In an axisymmetric model, vortex stretching cannot occur in all directions. Therefore, some upscale energy cascade may occur. RE noted that convection in Yamasaki's model (1977) resulted in the formation of a hurricane owing to upscale energy cascade. To minimize the possible upscale energy cascade, convection in the outer regions, supposedly in radiative-convective equilibrium, will not be simulated. Therefore, radiation is set to zero in the whole model domain. To be consistent, also the mean wind is set to zero in the whole model domain.

RE used an initial sounding that was neutral to the model's convective clouds. This sounding was created in the following way: The Jordan sounding (Jordan 1958) was used in the initial condition, and regions of convergence were prescribed in the model domain. No radiative cooling or surface fluxes were allowed. Convection occurs in the model, and after several hours the available energy for convection has been extinguished. In spite of using a different microphysical scheme than RE, I use the same neutral sounding that they used. The reason is that the creation of the neutral state involves **prescribed** forcing, in terms of convergence. The choice for the forcing is likely to affect the forming clouds and the resulting mean sounding more than just different microphysics.

Since the goal of the simulations, to be discussed in this chapter, is to test a hypothesis about the formation of hurricane Guillermo, we use a value for the Coriolis parameter that was taken from the mean latitude of the pre-Guillermo MCS, which is $12^{o}$N.

To test the hypothesis that evaporation of steady, mesoscale precipitation could lead to development of a moist vortex with a lower tropospheric cold core, a simple numerical experiment was designed. A steady mesoscale rainshaft is imposed, and any latent heating associated with the formation of this rain is neglected. In other words, a rainshower emanating from a prescribed altitude is switched on at the beginning of the simulation. There are neither wind nor temperature perturbations in the initial state of the model. However, a positive anomaly in the relative humidity is inserted in the upper troposphere with a maximum value of 80% to reflect the high relative humidity of the anvil, from which the precipitation would fall in a real MCS. The temperature is adjusted slightly so that the increase in humidity does not lead to an anomaly in virtual potential temperature. The rain water mixing ratio is set to 0.1425 $gkg^{-1}$ at 4.375 km altitude during the first 36 hours of the simulation. Also, the elevated relative humidity of 80% is maintained in the upper troposphere for 36 hours. The rainshaft extends to 116 km radius, outside of which the imposed flux of rainwater decreases linearly to zero over 37.5 km. These values are consistent with the observations from the system during flight 2P. The only exception is the rain rate. For the rain mixing ratio at 4.375 km altitude, we use a value that is 25% larger than the average mixing ratio in the stratiform rain at 3 km altitude during flight 2P. The average was calculated by converting radar reflectivity values to rainwater values and including all data with radar reflectivity less than 35 dBZ. No zero values were included in the averaging. The conversion relation was taken from Rogers and Yau (1989). The model does not have ice physics. Melting would deepen the layer of diabatic cooling by roughly a kilometer.

## 5.1 Control simulation

The development of the maximum tangential velocity in the control run above the lowest model level (625 m) and at the lowest level is shown in Figure 5.1. The initial vortex develops rapidly, but at 6 h the tangential wind under the rainshaft is still slightly anticyclonic at the lowest model level (Fig 5.2c). At 16 h the maximum cyclonic wind at the lowest model level is 4 $ms^{-1}$ (see also Fig. 5.3c). At 6 h the relative humidity has a positive anomaly above 2.5 km in the region of the rainshaft (Fig. 5.2b). The positive anomaly later extends to the surface within a 40 km radius (Fig. 5.3b), and the evaporation rate steadily decreases there. By 24 hours some shallow convection has developed about 35 km from the vortex center. At this time the maximum tangential wind at the lowest model level is 6 $ms^{-1}$.

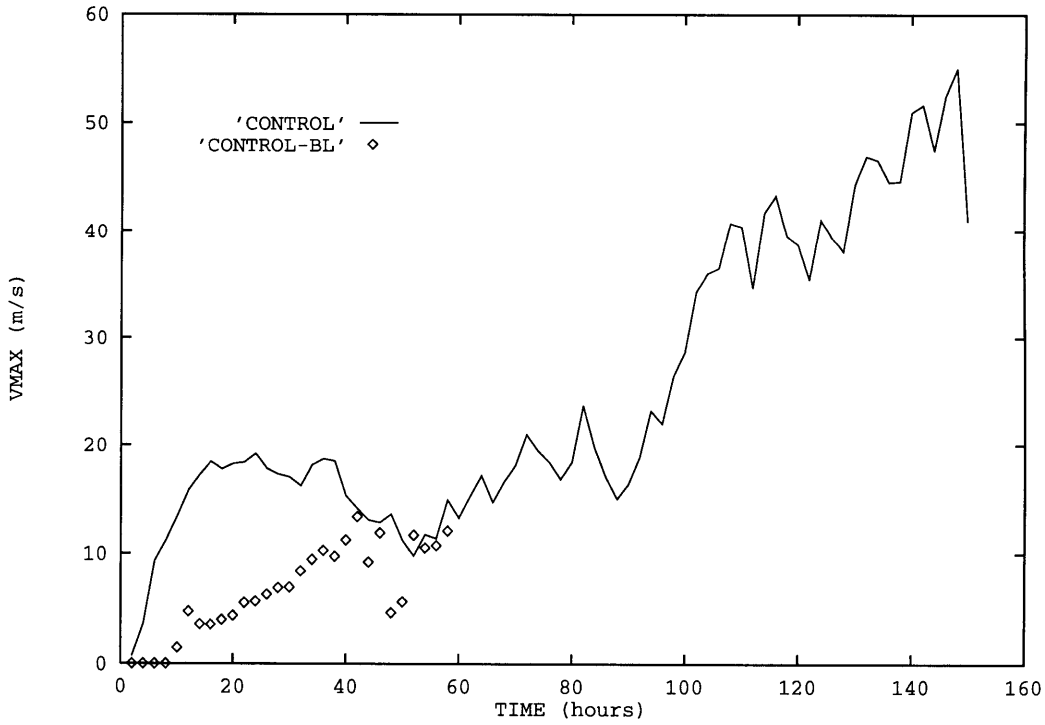


**Figure 5.1:** Maximum of tangential wind as a function of time above the lowest model level (solid); and at the lowest model level (diamond)

Deep convection develops by 48 hours at a radius of 60 km. By 60 h there is deep convection from 30 km to 260 km radius. The deep convection outside the inner 100 km develops and dies owing to downdrafts, while the deep convection within the inner 100 km is more persistent. However, angular momentum surfaces tilt strongly outward with height in the upper middle troposphere (not shown). This tilting is the result of the mid-tropospheric inflow during the time of the imposed rainshaft. Since convection tends to occur along angular momentum surfaces, precipitation falls into the inflowing air outside the main updraft. However, after 90 hours strong deep convection develops from 20 to 50 km radius, where the angular momentum surfaces are now nearly upright. Convection continues to occur in the same range of radius, and the system develops rapidly, whereas convection outside 100 km radius becomes sporadic and weak. The largest tangential velocity can be found at the lowest model level starting at 64 h. The vortex is still associated with a lower tropospheric cold core at this time, but the coldest temperature is not in the center anymore. At 96 h there is already a positive potential temperature anomaly in the center at the lowest model level.

It is somewhat surprising that shallow convection occurs in the middle of the rainshaft. When the rain is turned on, most cooling occurs at the top of the layer containing rain. The temperature anomaly at 6 h (Fig. 5.2a) is negative down to 2 km, and positive below. In the region of the positive temperature anomaly there is a negative anomaly in relative humidity (Fig. 5.2b). The positive temperature anomaly and the negative relative humidity anomaly are owing to subsidence below 2 km, forced by the evaporatively driven downdraft above. However, when relative humidity starts to increase within the inner 60 km above 2 km, there is more rain available within the lowest 2 km, and more evaporation occurs there. The warm and dry pool of air below the rainshaft close to the surface disap-

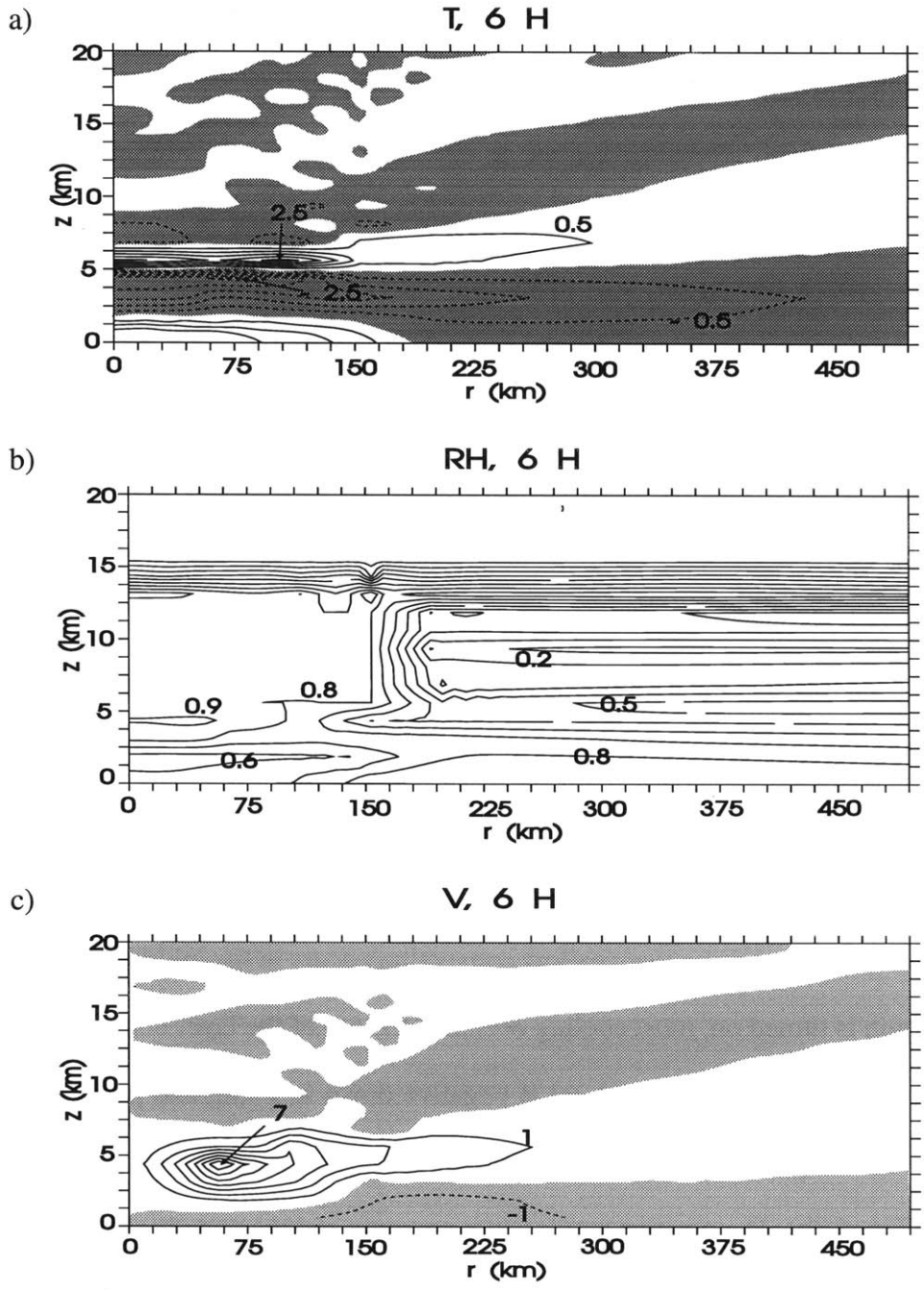


**Figure 5.2:** Average of (a) temperature anomaly (K), (b) relative humidity (percents), (c) tangential velocity ($ms^{-1}$), between 4 and 8 hours. Regions with negative values have been stippled.

pears (Fig 5.3 a and b), and the cold core extends to the surface within the inner 45 km. The extension of the cold core all the way to the boundary layer explains how shallow

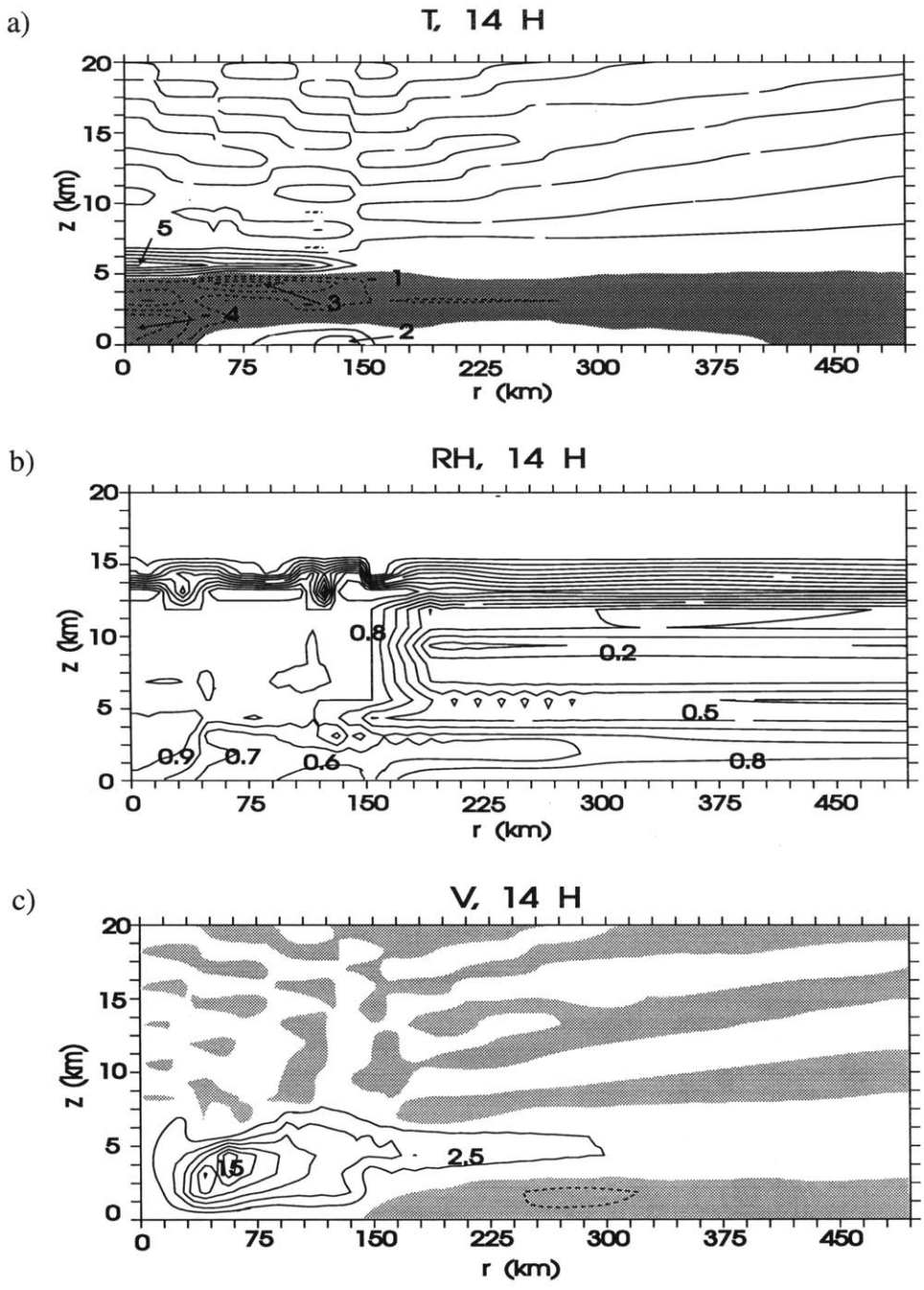


**Figure 5.3:** Same as in Fig. 5.2, but average calculated between 12 and 16 hours. Exceptionally, the negative values above 2.5 km have not been stippled in (a).

convection can develop in the middle of the rainshaft, when there is still a negative anomaly in the boundary layer $\Theta_e$ of several degrees. Namely, a decrease of temperature

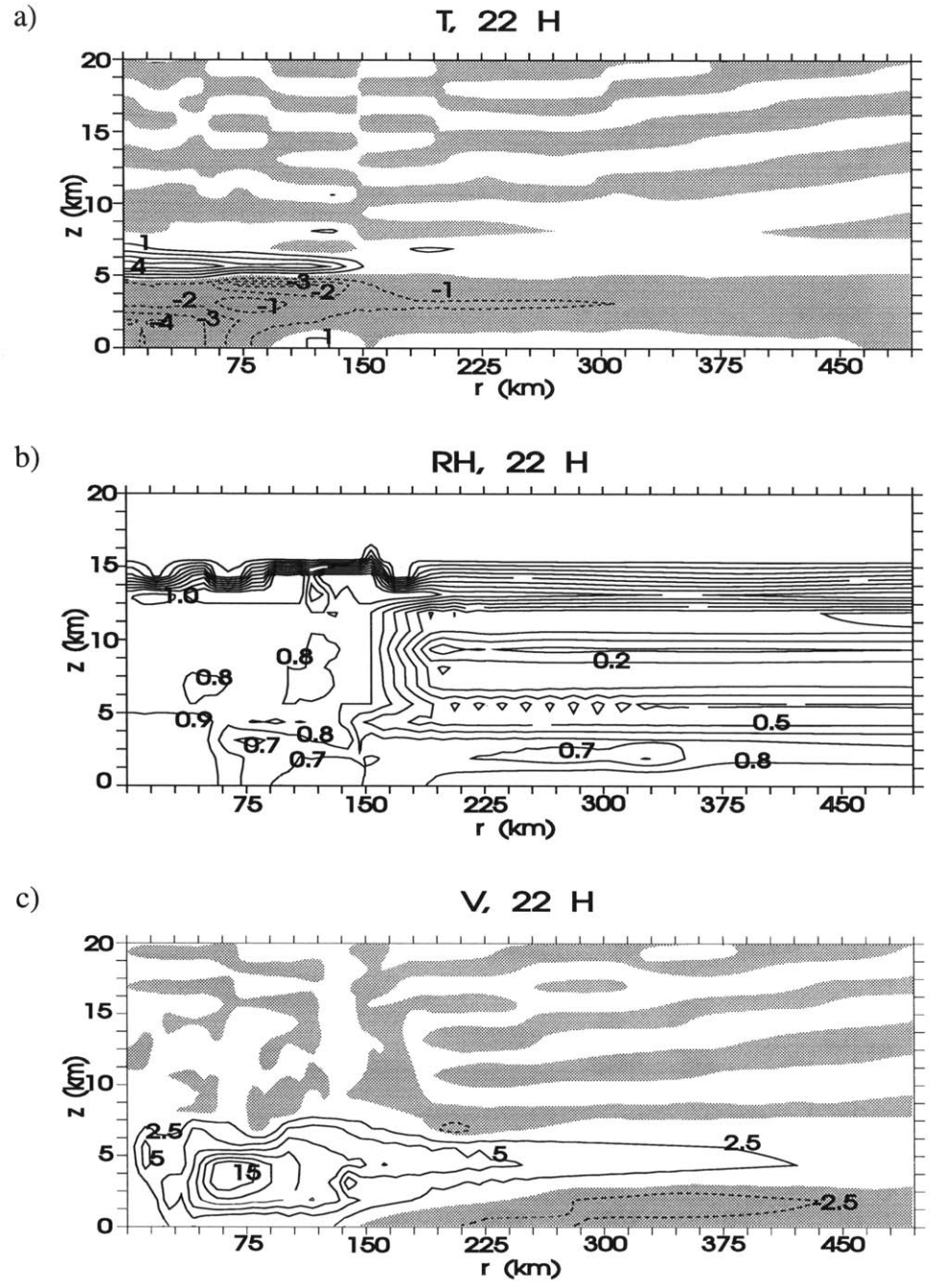


**Figure 5.4:** Same as in Fig. 5.2, but average calculated between 20 and 24 hours.

by 1 K, corresponds to a decrease in saturation $\Theta_e$ of 2.5 K for the appropriate temperature values. Therefore, a cold core is very efficient in reducing stability for shallow convection.

However, sea surface fluxes are also important for the development of the shallow convection. If surface fluxes are set to zero the developing shallow convection is weak. It should be noted that the sea surface fluxes depend only on the perturbation wind field since there is no mean wind in the model.

The flow is divergent in the boundary layer under the rainshaft. Initially the divergence leads to anticyclonic motion in the boundary layer (Fig 5.2c). However, vertical advection eventually increases cyclonic wind below the level of convergence (Fig 5.3c and 5.4c).[1] Note that between 14 and 22 h the radius within which the cold (and humid) core extends to the surface has doubled. Also, both the horizontal and vertical extension of the vortex have increased. However, the maximum wind speed has remained the same.

The presence of shallow convection, starting at 24 h, is likely to increase the tangential wind at the lowest model level owing to convergence to the shallow convection. The increase of tangential velocity can also be understood in terms of increase of potential vorticity, which increases below maximum heating (see equation 7.2). The moderate wind velocity in the boundary layer leads to increased sea surface fluxes, and finally at 48 hours deep convection develops.

The structure of the mature storm (Fig. 5.5) is remarkably similar to that of RE (their Fig. 5), only smaller in size. The hurricane strength winds extend only to 30 km radius. The size of the storm is comparable to that of Inez of 1966 (Hawkins and Imbembo 1976).

## 5.2 Sensitivity studies

The sensitivity of the model to several characteristics of the imposed rainshaft was tested. The initial conditions of the basic sensitivity studies are listed in Table 5.1. The maximum

1. The downward extension of the vortex will be explained in section 7.1 using the concept of potential vorticity.

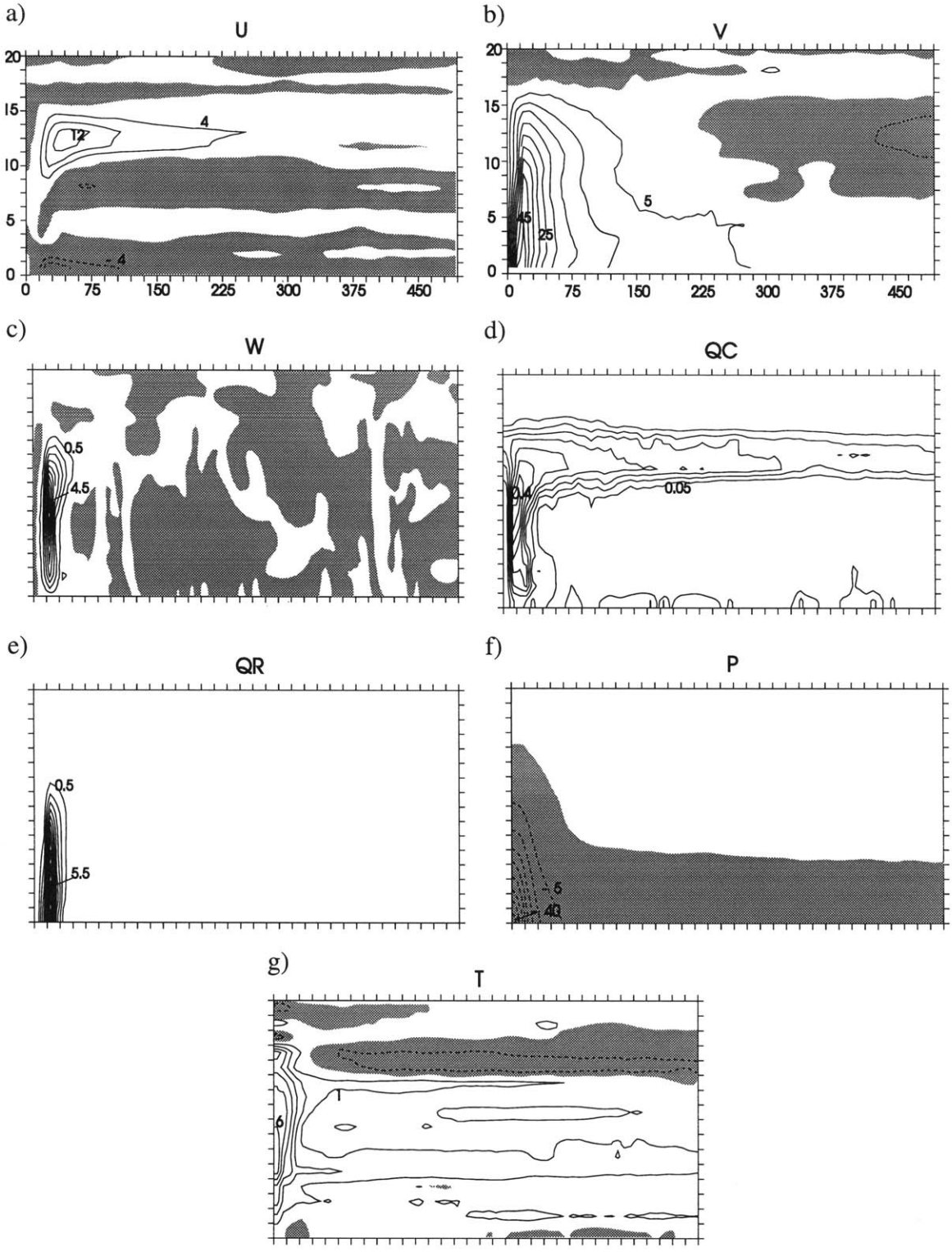


**Figure 5.5:** Hurricane in the control simulation. Fields averaged 125-150 hr. (a) Radial wind, (b) tangential wind, (c) vertical wind, (d) cloud mixing ratio, (e) rain mixing ratio, (f) pressure anomaly (hPa), (g) temperature anomaly (K). Unit for wind speed is $ms^{-1}$, unit for mixing ratio is $gkg^{-1}$. Negative values have been stippled.

tangential wind speeds from these sensitivity studies are shown in Figures 5.6 and 5.7.

The value of the rain mixing ratio of the imposed rainshaft was doubled in DMR and halved in HMR. After 50 h the maximum tangential velocity increases in DMR, whereas in HMR it decreases until 90 h, after which it starts to increase slowly. There are two main differences between the character of the convection in these experiments. First, in DMR deep convection develops between 20 and 30 h, but in HMR it takes 100 h for deep convection to develop. Second, in DMR deep convection first develops at 450 km radius, and the maximum vertical velocities between 20 and 60 h are generally found at a radius of more than 450 km, whereas in HMR deep convection is usually strongest within a few tens of kilometers from the center.

| Experiment | How differs from control run |
|---|---|
| DMR | q=0.2850 (double mixing ratio) |
| HMR | q=0.07125 (mixing ratio halved) |
| DA | $r_{rain}$=188 (double area of rain) |
| HA | $r_{rain}$=98 (area of rain halved) |
| HD | $\Delta t$=18 (duration halved) |
| HDDMR | $\Delta t$=18, q=0.2850 |
| HDDMR-FLUX | same as above but no surface fluxes for r > 340 km |

**Table 5.1: Model simulations. q is mixing ratio of the showerhead ($gkg^{-1}$), $r_{rain}$ is the radius of the showerhead (km), $\Delta t$ is the duration of the showerhead (h)**

In DMR there is more evaporation of rain than in the control simulation. Accordingly, the downdraft, anomalies in temperature and relative humidity are larger than in the control simulation. Even though the maximum tangential velocity is not much larger than in

the control simulation, the tangential velocity is larger in the boundary layer, and the positive anomaly there extends to larger radius than in the control simulation when the showerhead is switched off. Also, the outflow in the boundary layer is stronger than in the control simulation and it occurs at a lower altitude. This results in larger anticyclonic wind, and the larger wind speed close to the sea surface results in **increased sea surface fluxes also ahead of the outflow of low $\Theta_e$ air**. At 32 h the maximum anomaly of $\Theta_e$ in the boundary layer is 5 K in DMR and 2 K in the control simulation. The increased sea surface fluxes seem to be the reason for the convection developing at 450 km in DMR.

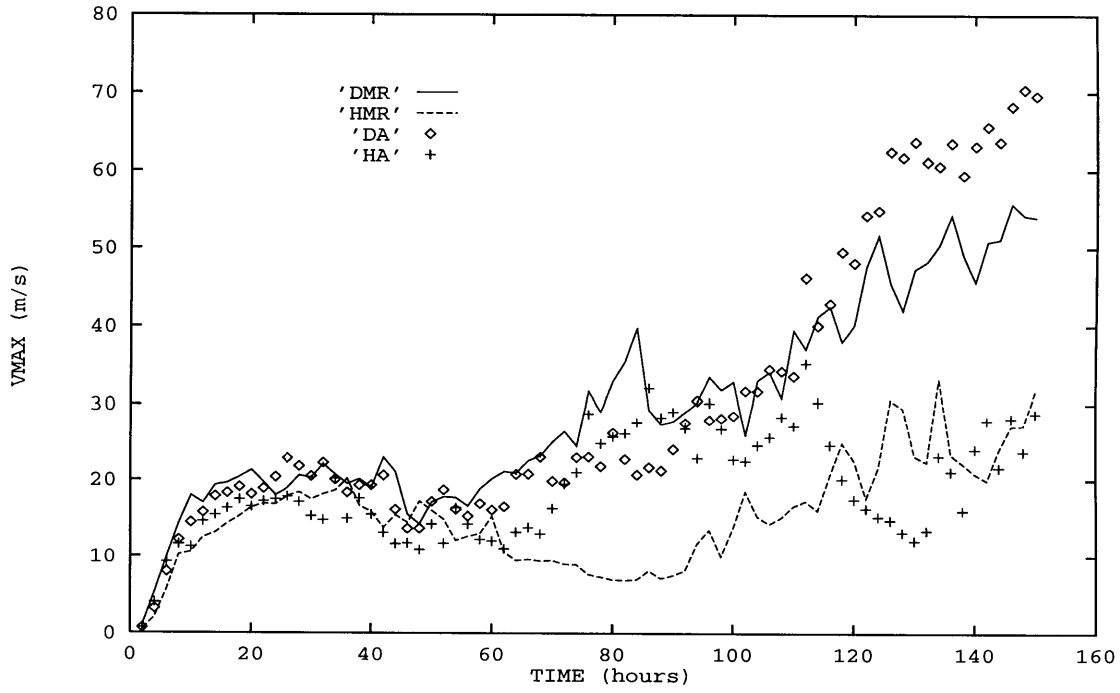


**Figure 5.6:** Maximum of tangential velocity as a function of time in experiments DMR (solid), HMR (dashed), DA (diamond), and HA (plus).

In HMR the boundary layer is drier and warmer than in the control simulation when the showerhead is switched off. The cold core is mainly above the boundary layer except

within the inner 70 km. In the control simulation the moist (in terms of relative humidity) cold core extends all the way to the boundary layer. The extension of the humid cold core and outflow to lower altitudes in the control simulation is likely owing to larger evaporation than in HMR, especially at lower altitudes.

Sensitivity to the areal coverage of the initial rainshaft was tested by doubling the rainshaft area in DA and halving it in HA. By the end of simulation time, the maximum wind speed in DA is about 20 $ms^{-1}$ stronger than in the control simulation, and in HA it is about 20 $ms^{-1}$ weaker. The initial development of the maximum tangential velocity is fairly similar in HA and DA. However, after 80 h the storm in HA becomes quasi-steady, and then weakens after 110 hours. The evaporation in DA induces anomalies of wind, temperature, and relative humidity over a larger area, and the wind anomalies are closer to the sea surface than in the control simulation. The outflow velocity extending over a larger range of radii results in larger anticyclonic wind, located closer to the sea surface than in the control simulation. Larger wind speed results in increased sea surface fluxes. As in DMR, outer convection develops. Once the outer convection weakens, the storm in the DA simulation starts intensifying. Meanwhile, the storm in HA does not suffer from convection occurring in the outer regions. However, the inflow within the lowest 2.5 km of low $\Theta_e$, which has not been replenished by the surface fluxes, causes the rapid weakening of the HA storm at about 110 hr. It could be that a higher horizontal resolution is needed to simulate HA properly. On the other hand, the magnitude of the negative anomaly of $\Theta_e$ is the same in HA and DA, whereas the wind speed is smaller in HA. This probably explains why $\Theta_e$ has not been replenished in HA.

Halving the duration of the rainshaft (experiment HD) results in slow development of the storm. The tendency of $\Theta_e$ at the lowest model level is hardly positive when the showerhead is switched off, apparently owing to small wind speed in the boundary layer (see

Fig. 5.3c). It should be noted that if the mean wind was accounted for in the model, the surface fluxes would be larger. It takes 72 hours before deep convection develops within a radius of 100 km. High values of $\Theta_e$ have not been replenished except in a small region close to the center, apparently owing to the small wind speed in the boundary layer. The weakening at 120 hours is associated with low $\Theta_e$ air flowing towards the center in the lower troposphere.

The observed MCS lasted, with changes in intensity of convection, from the early morning of 2 August 1991 until the vortex reached hurricane strength on 5 August 1991. Often MCSs last less than a day. In experiment HDDMR the duration of the rain was halved, and the strength of the rain doubled. The rain strength was doubled because, judging from satellite imagery, convective activity was at a minimum during flight 2P from

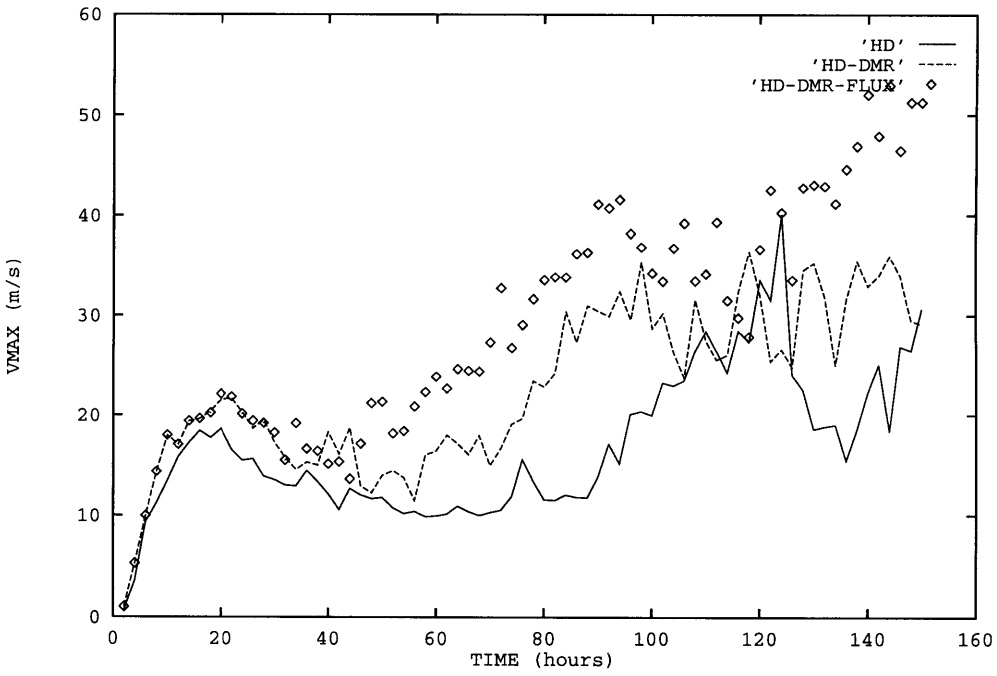


**Figure 5.7:** Maximum of tangential velocity as a function of time in experiments HD (solid), HDDMR (dashed), and HDDMR with surface fluxes set to 0 outside 340 km (diamond).

which the estimate of the rain rate for the control simulation was obtained. The development of the maximum value of the tangential wind is shown in Fig. 5.7. The maximum wind in the system reaches 30 $ms^{-1}$ by 80 h. Deep convection develops 450 km from the center after 20 h. Until the end of the simulation there is a tendency for convection to develop farther than 150 km from the center, and this convection often exceeds the inner convection in strength.

Based on sensitivity studies DMR, DA, and HDDMR, it seems that the outer convection can reduce markedly the rate of intensification. The outer convection seems to develop owing to increased surface fluxes associated with the outflow and anticyclone at the model's lowest level. To see the effect of the outer convection, we ran HDDMR anew, but with sea surface fluxes set to zero outside 340 km radius. No outer convection develops in this experiment. Without the outer convection a hurricane forms in 3 days, and reaches 50 $ms^{-1}$ maximum wind by the end of the simulation (Fig. 5.7). The result shows that the effect of the outer convection is clearly detrimental[1]. The strength of the outer convection may be at least partially an artifact of the absence of a mean background wind in the model. A mean wind of about 3 $ms^{-1}$ would probably be appropriate for a typical tropical boundary layer. If a radial or tangential wind velocity of 3 $ms^{-1}$ is added to the mean wind, the azimuthally averaged wind speed is 3.8 $ms^{-1}$, only 27% larger than the mean wind speed. Clearly this would not increase the sea surface fluxes as much as the increase of the wind speed from 0 to 3 $ms^{-1}$ would.

What role does the increased relative humidity in the upper troposphere above the rainshower play? To answer this question, two more simulations were run. Both are simi-

1. Note that the possible upscale energy transfer does not seem to be of a very important effect, since preventing the outer convection from occurring made the system develop faster.

lar to the control simulation except that in one of them the increased relative humidity of 80% is imposed only in the initial condition and is not maintained, as it is in the control simulation. In the other simulation the relative humidity is the same above the rainshaft as in the environment even in the initial state. The results (not shown) indicate that the development of the storm is not sensitive to the **maintenance** of the high relative humidity, but is somewhat sensitive to whether it is in the initial condition. If there is no increased relative humidity in the initial condition above the rainshaft, hurricane strength winds are reached about 40 hours later than in the control simulation.

Another set of experiments was made to test the sensitivity of the development to the initial humidity in the middle troposphere. The relative humidity in the lower troposphere, above the boundary layer, was increased to 77% in one experiment and decreased to 27% in another. The results are shown in Fig. 5.8. For the first two experiments model HDDMR-FLUX was used. The initial development in the experiment with the dry middle troposphere is much stronger, but by 120 hr the storm in the experiment with the moist middle troposphere is as strong as in the dry experiment. Initially, dryness of middle troposphere results in more evaporation and the resulting vortex is strong. However, towards the end of the simulation time it seems that the dryness of the environment is slightly detrimental for the system. One should treat these results with some suspicion, since one would assume that the environmental relative humidity could affect the outer convection, that was minimized in these two simulations by using a model version with no fluxes outside the radius of 340 km. However, the results are rather similar if the control model is used instead of the HDDMR-FLUX model, suggesting that the possible developing outer convection does not change the qualitative result that dryness of the midtroposphere is favorable for the initial development, but later development seems to be favored by a moist midtroposphere.

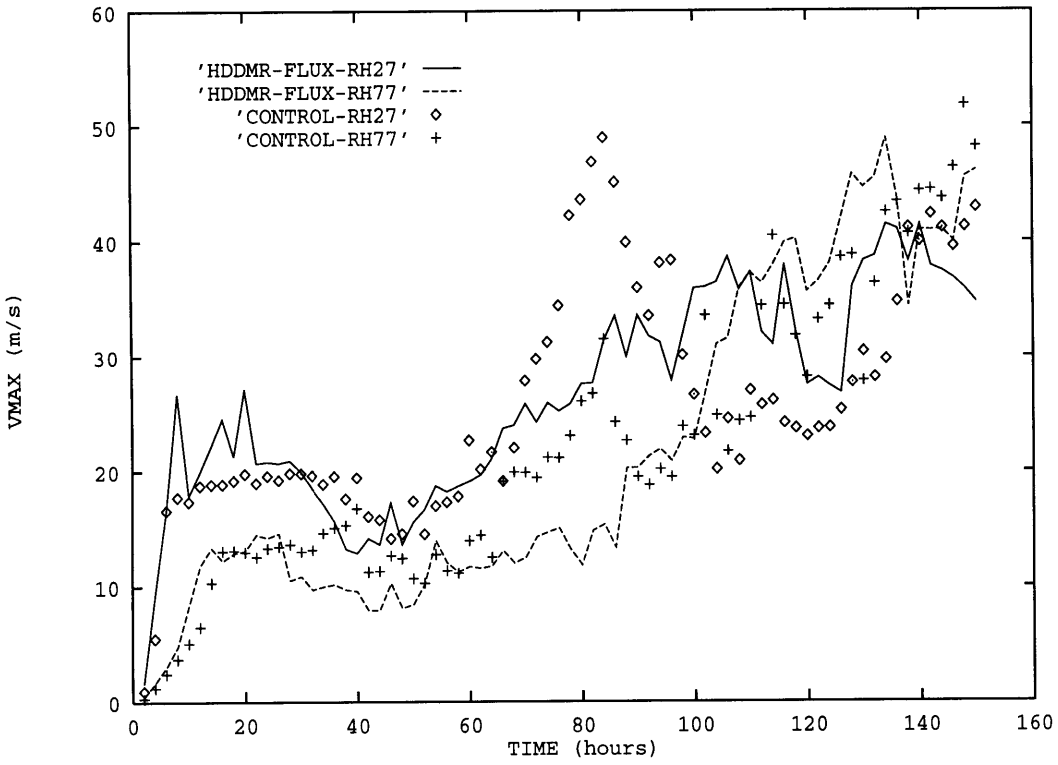


**Figure 5.8:** Maximum of tangential velocity in simulations with the HDDMR-FLUX model with low (solid) and high (dashed) middle tropospheric relative humidity; and with the control simulation model with low (diamond) and high (plus) middle tropospheric relative humidity

## 5.3 Comparison of the observations and the control simulation

The analysis of the pre-Guillermo system and the control simulation show many similarities. First, it takes about the same time (3-4 days) for the system to develop into a hurricane from the start of mesoscale precipitation. The model simulation shows high relative humidity in the core of the imposed rainshaft. High relative humidity was observed in the stratiform precipitation region on flight 2P. Also the cold core vortex is a common feature. Between the end of the imposed rainshaft in the model at 36 h and the rapid intensifi-

cation that starts after 90 h, a warm core develops within the lower tropospheric cold core (Fig. 5.9). The value of $\Theta_e$ has increased by several (4-5) degrees at the lowest level inside 150 km radius. Both the replacement of the cold core by a warm core inside a weakened cold core, and the increase of $\Theta_e$ in the boundary layer by several degrees were also observed to occur in the pre-Guillermo system between flights 2P and 4P.

It takes about 50 hours for deep convection to develop in the control simulation. On the contrary, satellite images do not show as long a time interval without cold cloud tops in the region of the MCS. This discrepancy might be owing to mean wind. Easterly mean wind adds to the vortex wind on the northern side, and would tend to favor convection there. The observations indeed show that convection is preferred on the northern side of the vortex center. This is also where the warm core is first observed.

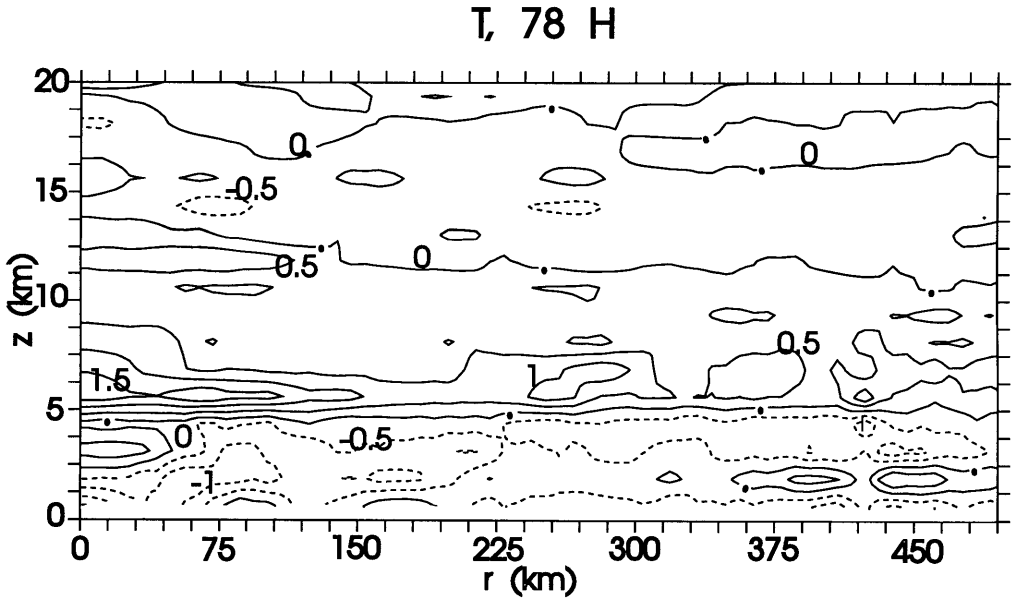


**Figure 5.9:** Temperature anomaly in the control simulation averaged between 76 and 80 hours. Negative values have not been stippled here but are shown with dashed contours.

# Chapter 6

# The roles of cold core vortices and relative humidity in cyclogenesis

Both in reality and in the control simulation, a tropical cyclone develops from a state with a cold core vortex and high relative humidity. To assess the relative importance of the high humidity and the cold core vortex, three simulations were run with simple initial disturbances. The initial conditions of these experiments are shown schematically in Fig. 6.1. Experiment B1 has high relative humidity in a mesoscale column but no vortex. Experiment B2 has high relative humidity and a cold core vortex. Experiment B3 has a cold core vortex without elevated relative humidity. In experiment B1 there is no wind in the initial condition, but the relative humidity is set to 100%, keeping virtual potential temperature constant, in a cylinder of 68 km in radius and extending from 2.5 km to 12.5 km altitude. In experiment B2 a cold core vortex was added to the initial state of experiment B1. The vortex has maximum tangential velocity of 9 $ms^{-1}$ at 3.1 km altitude. The maximum tangential velocity is reached at a radius of 64 km from the center, and the velocity vanishes at a radius of 338 km. The radial profile is the same as in RE. The velocity increases linearly with height up to 3.1 km, and above, it decreases linearly to zero at the base of the sponge layer. Temperature is decreased in the region with 100% relative humidity to conserve virtual potential temperature. In experiment B3 the same vortex is used as in experiment B2, but the mixing ratio of water vapor is horizontally homogeneous. In experiment B3 the anomalies of $\Theta_e$ and relative humidity are very small. In experiments B1 and B2 the anomalies of $\Theta_e$ in the middle troposphere are close to those observed on flight 2P. In all these experiments the wind velocity in the bulk aerodynamic formula was set to have a minimum value of 3 $ms^{-1}$ in the calculation of heat fluxes within 112.5 km radius. In

these simulations, the outer radius of the model domain was set to 1500 km, half of that used in other simulations.

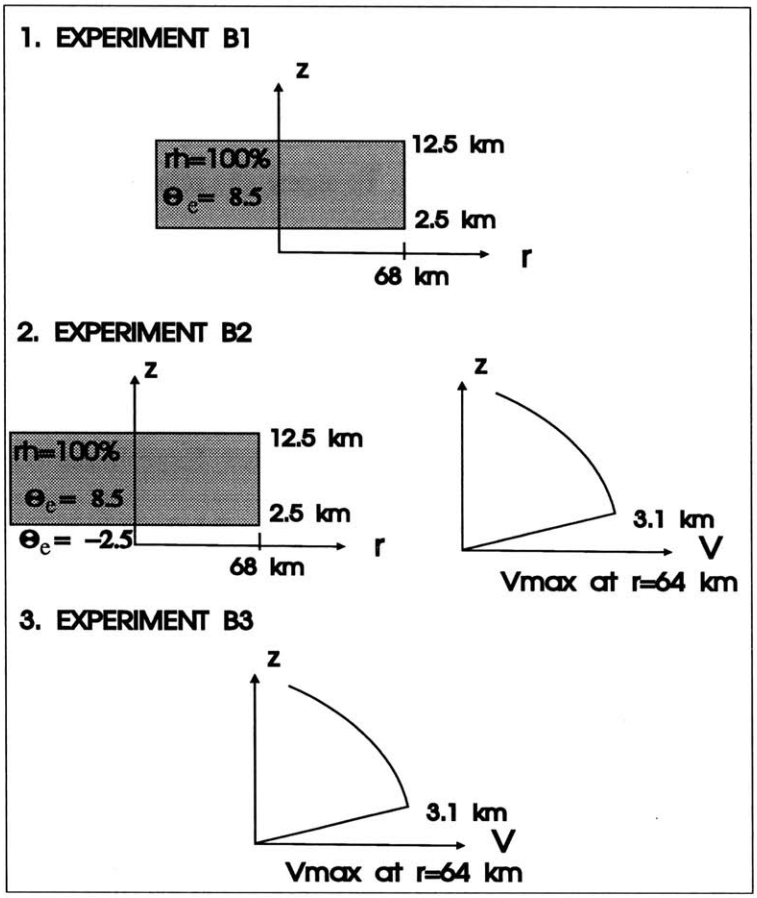


**Figure 6.1:** Schematic illustration of initial conditions in sensitivity experiments. See text for details.

The maximum tangential velocities in B1, B2 and B3 are shown in Figure 6.2. In experiment B1 convection develops within hours. But inflow above the boundary layer decreases relative humidity and downdrafts develop. The value of $\Theta_e$ decreases remarkably in the boundary layer, suppressing convection. The system fails to intensify by 150 h. This is in contradiction with simulation results of Emanuel (1995) showing that saturation of a mesoscale column is a sufficient condition for cyclogenesis. The discrepancy is likely

owing to the different scale of the moist column. In our simulations it is 68 km in radius. In Emanuel's study it is 150 km in radius. It should be noted that the moist column in the data from flight 2P (Fig. 3.5a), with close to 90% relative humidity, is about 50 km in radius, and in the control simulation 90% relative humidity extends to 70 km in radius when the showerhead is switched off. Experiment B3 was run anew but with the moist column extending to 150 km. By the end of this simulation the system is a marginal hurricane, confirming Emanuel's result that **a large enough** column of **saturated** air can result in a hurricane in the presence of a wind perturbation of only 3 $ms^{-1}$.

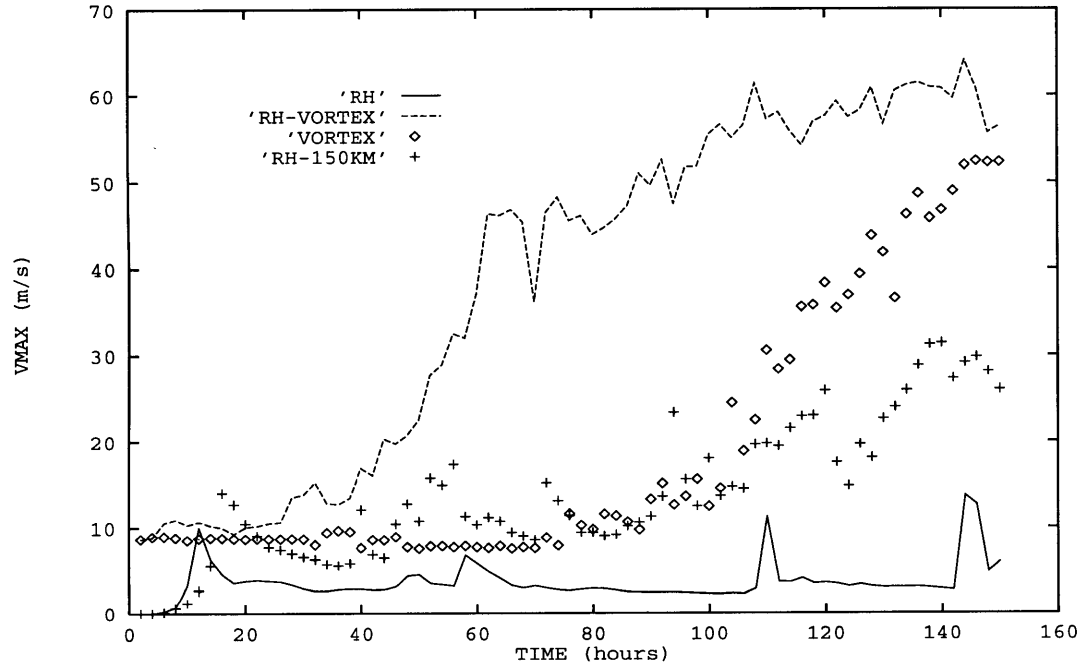


**Figure 6.2:** Maximum of tangential velocity as a function of time in experiments B1 (solid), B2 (dashed), B3 (diamond), and in experiment with moist column extending to 150 km (plus).

In experiment B2 convection also develops within hours. There is initially as much cooling by evaporation in experiments B1 and B2. However, convection does not cease in

B2. There are two possible reasons for this. First, at 16 h $\Theta_e$ is small in both experiments, but experiment B2 shows more conditional instability because the cold anomaly of about 3 K in the lowest few kilometers implies a negative anomaly of saturation $\Theta_e$ of about 8 K. Second, in B1 there is strong inflow at midlevels feeding convection. This inflow extends all the way to the inner core of the system. There is no such strong inflow in experiment B2, perhaps owing to increased inertial stability.

Experiment B3 shows that without the high relative humidity, development of the initial cold core into a hurricane is delayed by two days owing to larger evaporation of rain and cloud, and stronger downdrafts. Even though the downdraft air in experiment B3 has remarkably smaller $\Theta_e$ than in experiment B1, the disturbance in experiment B3 develops more rapidly than in experiment B1. Therefore, it does not seem to be the case that the favorable effect of the initial cold core vortex is owing to reduction of the inflow of low $\Theta_e$ air by the enhanced inertial stability. The fact that B3 develops only 2 days later than B2 suggests that in the presence of a cold core vortex, with tangential wind speed increasing from 0 to 9 $ms^{-1}$ within the lowest 3 km, the initial dryness of the middle troposphere cannot prevent the system from intensifying.

The wind associated with the initial cold core cyclone in B2 and B3 was made to decrease to zero at the bottom of the sponge layer, which lies at 24 km altitude. Another set of simulations in which the cyclonic winds were made to decrease to zero at 17 km showed qualitatively similar results.

In a summary, the vortex seems to be more important for the development than the high relative humidity for the chosen model configuration. However, high relative humidity can make the cyclogenesis occur faster.

# Chapter 7

# Discussion

The numerical experiments discussed in Chapter 5 were intended to explore the formation of a cold core mesoscale cyclone by evaporation of mesoscale precipitation from a preexisting MCS. The effects of deep convection associated with the initial MCS were neglected. Deep convection would result in a flux of low $\Theta_e$ into the boundary layer that is now missing from the model. On the other hand, there is no mean wind in the model either. Mean wind would increase the fluxes of heat and moisture from the sea surface in the region of the MCS.

The rainshower in the control simulation extends to 116 km in radius and the imposed rain flux then declines linearly to zero in 37.5 km. It is interesting to note that over the western tropical Pacific 1% of the cloud systems whose areas are defined by the 208 K infrared temperature threshold have been observed to exceed 50 000 square kilometers in size, corresponding to 126 km in radius (Houze 1993, p. 337). The 208 K threshold is often used for correlating infrared temperatures with precipitation. Houze (1993) notes that these large cloud systems account for almost 40% of the total area covered by clouds with this temperature threshold.

The duration of rain from the pre-Guillermo MCS was rather long. The control simulation shows that after 36 hours of independent precipitation, the system is able to produce its own precipitation. Even 18 hours of precipitation is enough for this to happen in the model. One of the questions not answered in this study is: what is the longevity and size of precipitation needed in the presence of radiation, mean wind, large-scale forcing, and deep convection? To answer this question one should use a three-dimensional model and be able to understand and simulate the formation of an MCS. Another interesting question is:

How would the presence of a weak large-scale vortex affect the outlined mechanism? I ran the control simulation discussed in Chapter 5, with a slight modification. Namely, I added to the initial condition a weak warm core vortex, with maximum tangential wind of 5 $ms^{-1}$ at 270 km radius. The results show that the hurricane develops about a day earlier with the weak vortex. Otherwise, the development is fairly similar to the control case. If the model is run with the weak vortex but without the imposed rainshaft, no hurricane develops by 150 h. By the end of the simulation the maximum tangential velocity is only 10 $ms^{-1}$.

## 7.1 Thought experiment on the downward propagation of vorticity

The simulations of Chapters 5 and 6 suggest that a mesoscale cold core vortex is an ideal embryo for tropical cyclogenesis, provided it extends downward into the boundary layer. If the cold core vortex does not extend to the boundary layer by the time the rainshower is switched off, a cyclone develops very slowly, if at all (simulation HD and Figures 5.2, 5.3,and 5.4). The vortex winds are important for sea surface fluxes, vorticity is associated with a decreased Rossby radius of deformation, and the cold core right above the surface enhances convection because every degree of negative temperature anomaly is associated with a 2.5 degree anomaly in saturation equivalent potential temperature. And convective instability depends roughly on the difference between boundary layer $\Theta_e$ and the value of saturation equivalent potential temperature above. Therefore, the cold core also diminishes the role of downdrafts in preventing further convection. The downward development of the cold core vortex as a direct result of evaporation (maybe also melting and water loading in practice) may be of crucial importance to tropical cyclogenesis. In this section I offer a few speculations about how the downward development of the vortex may occur based on a simple thought experiment. I also suggest what might prevent the downward development.

The thought experiment concerns changes of potential vorticity of parcels experiencing diabatic cooling. Potential vorticity and its conservation equation are (see Hoskins et al. 1985):

$$PV = \frac{1}{\rho}\vec{\zeta}_a \bullet \nabla\Theta \tag{7.1}$$

$$\frac{d}{dt}PV = \frac{1}{\rho}\vec{\zeta}_a \bullet \nabla\dot{\Theta} + \frac{1}{\rho}\vec{K} \bullet \nabla\Theta\,, \tag{7.2}$$

where vector $\zeta_a$ is the absolute vorticity, and vector K is the curl of frictional force. For simplicity, we neglect friction here. Hence K equals zero. Assume that the horizontal component of (relative) vorticity is zero, and that the vertical component is constant. In that case, the Lagrangian derivative of potential vorticity (PV) depends only on the vertical gradient of diabatic heating. Let us switch on constant diabatic cooling in a mesoscale region, depicted in Fig. 7.1. Once the cooling is switched on, the parcels that go through the upper boundary of the cooling region experience an increase of PV of some amount. The parcels that go through the lower boundary of the cooling region must experience a decrease of PV of the same amount. This result can be understood in terms of the conservation of mass-weighted PV over a material volume. Namely, integrated over a fixed material volume of air, the mass-weighted integral of potential vorticity must be conserved if the dot product of the gradient of the diabatic heating and vorticity is zero at the boundaries of the material volume. (The conservation of mass-weighted PV over a material volume can be readily derived from the PV conservation equation, see Hoskins et al. 1985 for details.)

Soon there will be a positive PV anomaly within the region of cooling, and a negative PV anomaly below it. When the parcels that went through the upper boundary of the cooling region reach the lower boundary they will lose their positive PV anomaly and emerge with no PV anomaly. This applies to a linear problem[1].

The initial negative PV anomaly gets dispersed, with divergence below the cylinder (Fig. 7.1b). The cylinder has a positive PV anomaly and directly below there is no PV anomaly. In the vorticity field one would expect a cyclone to dominate the wind field below the diabatic cooling. The time it takes for the first parcel that went through the upper boundary of the cooling region to reach the lower boundary can be used as a rough estimate for the time it takes for the negative PV anomaly to disappear from directly below the layer of cooling. For a depth of the layer of 4000 m, and vertical velocity of 0.1 $ms^{-1}$, the time scale is 10 hours. The vertical velocity of 0.1 $ms^{-1}$ was chosen based on the estimate of the downdraft velocity of 0.06 $ms^{-1}$ in the stratiform region of a tropical squall line (Gamache and Houze 1982).

We noted before that in the control simulation, the relative humidity increases in the layer between 2-4 km, and this results in more precipitation and thus an enhancement of evaporation within the lowest 2 km. In terms of the thought experiment, the cylinder of cooling descends to lower altitudes. In the control simulation this occurs in the same time

---

1. To be precise, if there is *increase of the rate* of production and destruction of PV *while* a parcel is in the layer of cooling, it will have a negative anomaly after it has come out of the layer. In a non-linear problem, the vorticity generally increases with time Therefore, the PV production rate also increases steadily with time. If vorticity is relatively homogeneous in the cooling region, there will be a large mass of air with small magnitude of a negative PV anomaly below the cooling region, and a small mass of air with large positive PV anomaly in the cooling region. It has to be noted that the parcels coming out of the layer of cooling will diverge horizontally. Hence, the negative PV anomaly is spread to a large horizontal area.
As soon as relative vorticity starts to change, the source of PV at the upper boundary has to be slightly larger than the sink at the lower boundary. Since the integral of the mass-weighted PV over a material volume is conserved when there is no diabatic heating at the boundaries of the material volume, there has to be destruction of PV somewhere else than just at the lower boundary. The additional destruction occurs at the horizontal boundaries of the region with cooling.

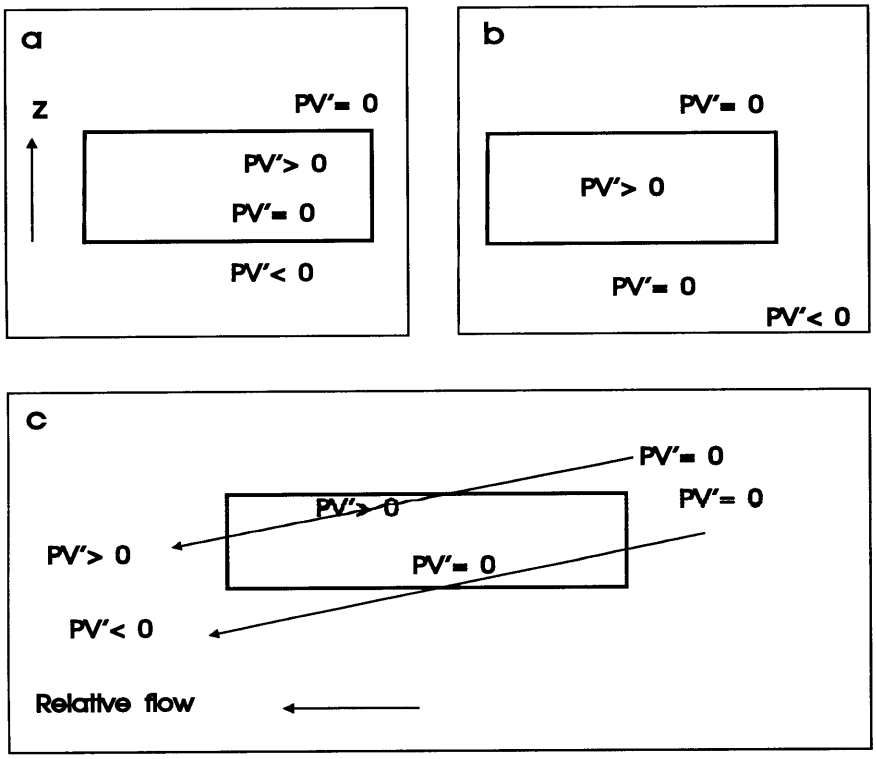


**Figure 7.1:** Thought experiment of cooling in a cylinder. PV anomalies (a) after parcels descended half of the depth of the cylinder; (b) after parcels descended the whole depth of the cylinder; (c) with relative flow, arrows show hypothetical trajectories. In (a) and (b) PV anomalies are symmetric about the vertical axis of the cylinder.

as it takes a parcel to descend 4 km. Both the dispersion of the negative PV anomaly while the positive PV anomaly is confined to the cylinder, and the downward movement of the cylinder of cooling is expected to affect the development of the vortex downward. Note that if the rain rate is larger, the cylinder of cooling is deeper to start with, and the parcels travel faster to the lower boundary of cooling. Therefore the downward development of the cyclone can be expected to occur sooner. This is consistent with the results from experiment DMR.

Apart from the strength and duration of rain that may be important for the downward development, a relative flow through the system (for example owing to environmental shear or owing to the system's internal dynamics) could also be important. The situation with a relative flow is shown in Figure 7.1c. Those parcels that go through the upper boundary of cooling but not through the lower boundary will retain their positive PV anomaly. Those parcels that go through the lower boundary but not through the upper boundary will retain their negative PV anomaly. Note that in this case the positive (and negative) PV anomaly will be diffuse. Thus vorticity will not increase within the volume of cooling as much as it would without the relative flow through the system. This will make further changes of PV smaller, since PV production is proportional to vorticity. In this case one would expect to see a weak cyclone above a weak anticyclone.

It is remarkable that even though squall lines have been observed to produce midlevel cyclones, there are no instances known to the author of tropical cyclogenesis from squall line-produced midlevel cyclones, whereas MCS-produced cyclones often lead to cyclogenesis. This may be owing to two factors. First, the time it takes for a parcel to descend through the layer of stratiform precipitation may be larger than the time the stratiform rain lasts in squall lines. This, in turn, might be owing to the short duration of precipitation and/or weak precipitation leading to weak downdraft. It is interesting that Gamache and Houze's (1985) analysis of a tropical squall line indeed shows that a cyclone resides in the middle troposphere with negative relative vorticity below it. Second, a relative flow through the system may explain why in many squall lines the midlevel cyclone may be weak if it exists at all.

It is worth noticing that a relative flow through the system may not only be owing to shear. For example in case of an atmospheric wave there is relative flow through the wave,

even without shear. A tropical cloud cluster "tied" to a wave may experience too much relative flow to be able to spawn a tropical cyclone.

We neglected friction in the thought experiment. However, it has an important role in the further intensification of the system. In the absence of surface friction air in the boundary layer would keep its negative PV anomaly. Once convective heating commences in the vicinity of the cold core vortex, air with a negative PV anomaly would converge towards the vortex in the boundary layer. However, surface friction increases PV if wind is anticyclonic (equation 7.2). Therefore, surface friction decreases the magnitude of the negative PV anomaly in the boundary layer.

## 7.2 Importance of the outlined process for cyclogenesis in practice

The case studies referred to in the introduction suggest that tropical cyclogenesis may start when a mesoscale vortex forms in a MCS. However, it is not known how often tropical cyclones form in this way. Further, in those studies it was noted that the mesoscale vortex is initially strongest in the middle troposphere. The present study suggests that the downward propagation of the vortex and the replacement of the cold core by a warm core occurs only when there has been enough diabatic cooling so that the cold core extends to the boundary layer. However, it has been suggested by Chen and Frank (1993) that the downward propagation of the vortex occurs as the anvil cloud grows downward. There are two studies that may shed light on these two questions. Both studies were made by Zehr. The other one is a composite study using radiosonde data, and the other one is a study using satellite data. In both studies data were gathered from many cases of cyclogenesis.

Zehr (1976) studied tropical cyclogenesis over the western Pacific by comparing rawinsonde data composited with respect to pre-typhoon and non-developing tropical cloud clusters. Data sets 0 and 00 are for nondeveloping cloud clusters. Data set 00 is a subset of

dataset 0, restricted to the months of June through September and limited to certain locations in the western Pacific. Sets 1 and 2 are for developing cloud clusters, 2 being later than 1 in the sequence of development. Since the data is composited according to its distance from the disturbance center, the location of the center had to be determined. Zehr notes that the major source of error in the composites is the uncertainty in positioning of the disturbances, which is mainly based on satellite imagery. The average radius of the cloud clusters is 1.5 to 4 degrees in latitude, and the compositing is done with respect to 2-degree latitudinal rings.

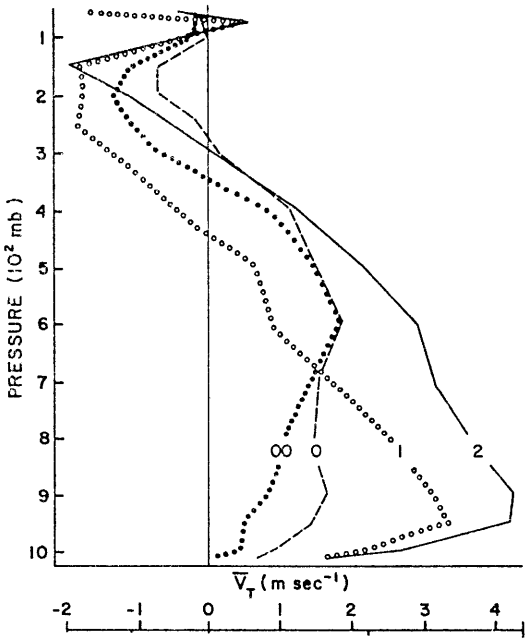


**Figure 7.2:** Vertical profile of tangential wind in the 1-3 degree band surrounding the center of the cluster (Zehr 1976)

In Fig. 7.2 the vertical profile of tangential wind is shown in the 1-3 degree band around the center of the cluster. Tangential velocity increases below 600 hPa in data sets 0

and 00. In data set 00 the velocity increases from 0.5 $ms^{-1}$ at 950 mb to almost 2 $ms^{-1}$ at 600 hPa. This suggests that the nondeveloping clusters have a lower tropospheric cold core. This conclusion is consistent with the thermal anomalies in the nondeveloping clusters shown in Fig. 7.3. The difference of the temperature within the inner 3 degrees and a band from 5 to 7 degrees is shown in Fig. 7.3b. It should be noted that since the mean cluster radius is from 1.5 to 4 degrees, the inner 3 degrees must be well resolved.

The situation is more complicated in the case of developing clusters. In data sets 1 and 2 tangential velocity decreases with altitude in the ring between from 1 to 3 degrees (Fig. 7.2), suggesting a warm core. The temperature difference between the inner 1 degree and the ring between 5 and 7 degrees is shown in Fig. 7.3a. It should be noted that it may be difficult to determine the center of the system to within one degree. However, the inner 1 degree seems to be warmer than the ring between 5 and 7 degrees above 880 hPa. This is consistent with the change of tangential velocity with altitude. However, Fig. 7.3b shows that in these clusters air is colder within the inner 3 degrees than in the ring between 5 and 7 degrees in the layer below 680 hPa. **These observations together suggest a reversal in temperature gradient somewhere within the inner 3 degrees in the developing clusters, with a warm core inside a cold core.** Indeed, this is true of pre-Guillermo and the control simulation as well. The reversal of temperature gradient was observed in pre-Guillermo during flights 4P and 5E, and until 80 hours there is a reversal of temperature gradient in the control simulation.

Turning our attention back to the nondeveloping cases, there is an important piece of information we have not yet considered about the vertical temperature structure of the nondeveloping cases. This the fact that **the nondeveloping clusters' lower tropospheric cold core, best defined between 600 and 700 hPa, almost changes to a warm core around 800 - 920 hPa. The same is not true about the developing clusters (Fig. 7.3b).**

**This structure observed only in the nondeveloping clusters supports our conclusion, based on the sensitivity studies, that the extension of the cold core through the whole lower troposphere to the top of the boundary layer is needed for cyclogenesis to occur.** Note that a cold core above a warm core was observed in the control simulation at 6 hr (Fig. 5.2).

The nondeveloping clusters show a colder anomaly within the lowest 30 hPa than the developing clusters. The cold pool in the boundary layer is probably owing to convective downdrafts associated with deep convection. The higher wind speed in the boundary layer (Fig. 7.2) associated with the developing clusters may explain why the cold anomaly is weaker in the developing clusters than in the nondeveloping clusters.

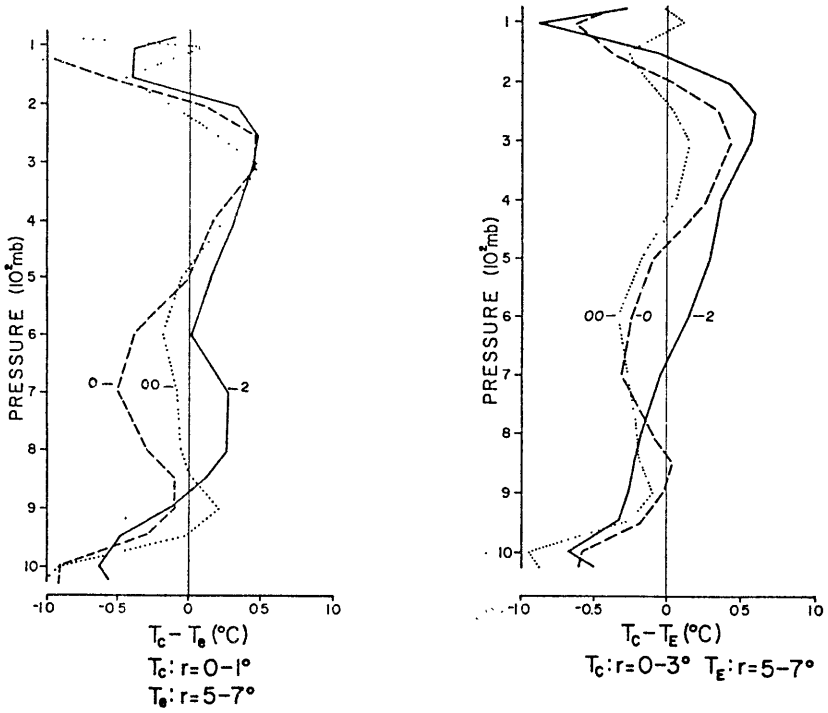


**Figure 7.3:** Thermal anomalies in the clusters. Difference of temperature within the inner (a) 1 degree and environment, (b) 3 degrees and environment. Environment is defined here as the 5-7 degree band around the center of the cluster (Zehr 1976).

To estimate the ventilation (i.e. flow through the system) the mean u-component of the wind in the inner 3 degrees and the mean motion of the disturbance is shown in Fig. 7.4. Zehr notes that the mean meridional wind is small, and propagation is mainly to the west.

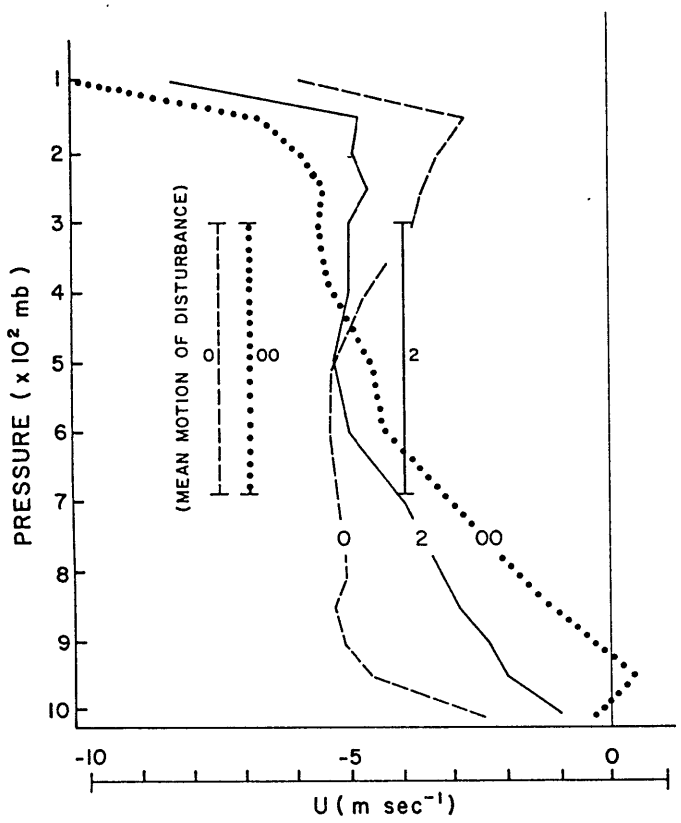


Fig. 23. Zonal wind or u-component of the wind. The mean values of u in the r = 0°-3° region are plotted for the pre-typhoon (2) and non-developing (0 and 00) clusters. The mean u component of the propagation vector is also depicted.

**Figure 7.4:** Vertical shear in the clusters, and the mean motion of the clusters (Zehr 1976).

Note that the average magnitude of the shear is always underestimated owing to the averaging, and the underestimation depends on how variable the direction of the shear is. In data set 00 large shear is obvious in the lower troposphere. Data set 0 would seem to have very small mean shear, but Zehr notes that the vertical profile of zonal wind for dataset 0 is an average of a large number of zonal wind profiles with considerable variability. Therefore, the small shear in Fig. 7.4 may just be an artifact owing to cancelling directions of the shear vector. However, it is clear that both the shear and the difference between the

zonal mean wind and the mean motion of disturbance is large in data set 00, and the latter is especially large in the lower troposphere where one would expect the evaporation effects to dominate. The shear appears to be as large in data set 2 as in data set 00. However, in data set 2 the difference between the mean zonal velocity and the propagation of the system would appear to be remarkably smaller than in data set 00.

We have now found evidence that cases of tropical cyclogenesis over the western Pacific show a warm core inside a cold core, and that non-developing cases do not have the cold core extending to the boundary layer. These observations support the theory outlined in this work for tropical cyclogenesis from mesoscale systems. However, these qualitative results are not inconsistent with the simulations of Chen and Frank. Namely, the intensity of the cold core might just reflect how much condensation there has been in the anvil cloud. However, the second study by Zehr supports the theory outlined in the present work.

In the second study, Zehr studied again tropical cyclogenesis in the western North Pacific. In this study he used satellite images to characterize convection in cyclogenesis. Convection was associated with cold infrared temperature thresholds using 3-hourly GMS satellite data. Zehr found that tropical cyclogenesis was typically characterized by an early convective maximum, which precedes the initial appearance of a tropical depression. The early convective maximum was defined objectively by estimating the percentage of the area within 2 degrees from the center of the cloud cluster with infrared temperature less than -65 C. The early convective maximum occurs at the time of maximum coverage of cold infrared temperature, provided that 1) it precedes the designation as a tropical depression, and 2) a 24 hour period including this maximum has a greater area than the 24 hours following it. 80% of tropical cyclones were observed to have an early convective maxi-

mum. Using visible images, he found that a mesoscale vortex is often the result of the convective maximum. An example of the early convective maximum is shown in Fig. 7.5.

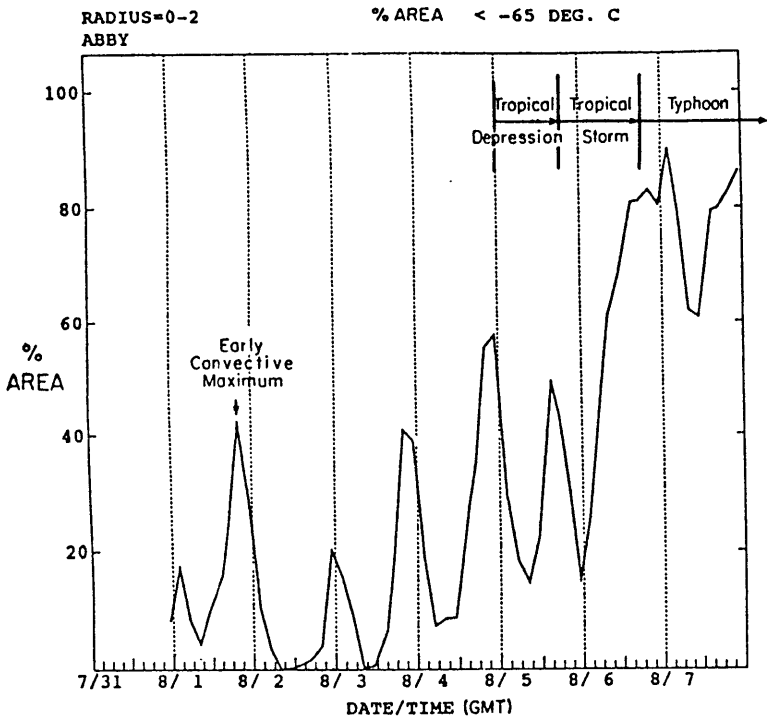


**Figure 7.5:** Early convective maximum of Typhoon Abby, 1983. The percentage of area within inner 2 degrees with infrared temperature less than -65 K is shown as a function of time (Zehr 1992).

Zehr notes that before the early convective maximum there is little or no curvature in the deep convective cloud bands, or no bands at all. After the convective maximum, a well-defined, persistent, cyclonic curvature in the deep clouds appears. The early convective maximum and associated mesoscale vortex formation preceded the first designation as a tropical storm by an average of 3 days. The first substantial decrease in central sea-level pressure occur only at a later stage of tropical cyclogenesis.

What do these observations tell us about cyclogenesis? First of all, the fact that convection is suppressed after the early maximum (usually by about 2 days or more) tells us that either the forcing for convection has decreased, or that boundary layer $\Theta_e$ has been decreased by downdrafts. The latter indeed seems to have happened in pre-Guillermo. We noted that the most important thermodynamic change that took place between flights 2P and 4P was the increase of $\Theta_e$ in the boundary layer. It also seems that convection was somewhat suppressed after the initial eruption that took place before flight 2P, and before flight 4P. The decrease of the magnitude of convection is not expected if the anvil cloud is growing steadily downward in a moist environment, which can support convection with primary inflow occurring at midlevels.

Another interesting result from Zehr's study is that after the first convective maximum, convection becomes more concentrated in space. In the case of predominantly warm core and small surface wind anomaly, one would not expect to see the concentration of convection.

In a summary, Zehr's results suggest that the development of a lower tropospheric cold core vortex, with the cold anomaly extending through the lower troposphere to the boundary layer, is the key process in tropical cyclogenesis over the western Pacific. The suppressed convection after the early convective maximum may be owing to the need to replenish (partially) the boundary layer $\Theta_e$.

# Chapter 8

# Concluding remarks

The vortex in the pre-Guillermo mesoscale convective system was initially found in the stratiform precipitation region of the MCS. There was a positive anomaly of relative humidity and a negative anomaly of virtual potential temperature in the vicinity of the vortex at 3 km altitude. A negative anomaly of virtual potential temperature was also found in the boundary layer. On flight 4P, 28 hours later, a small-scale positive anomaly of virtual potential temperature, inside the negative anomaly, was found collocated with convection. This structure in the temperature field was found both at 3 km and in the boundary layer. By flight 5E, 14 hours after flight 4P, wind speed had increased, and the system had a lower tropospheric warm core.

Numerical simulations with an axisymmetric model show that precipitation lasting for 36 hours and covering enough area results in a humid vortex with a lower tropospheric cold core. A hurricane develops in 3 days in the model. Decreasing the rain rate or the duration of the rain results in markedly slower development. If precipitation lasts for only 18 h, but is doubled in strength, a hurricane results, but it is less strong than in the control case. This is owing to the development of convection several hundred kilometers from the center. It is not possible to say whether the outer convection would develop were the radiation and mean wind accounted for. Numerical experiments with idealized initial disturbances show that the existence of the initial cold core vortex is crucial to the further development of the system; high relative humidity by itself does not lead to development unless it occupies a fairly large volume. However, the existence of a **midlevel** vortex is not enough. A sensitivity study with halved duration of the rainshower suggests that cyclo-

genesis can be prevented if the cold core vortex does not extend to the boundary layer when rain is stopped.

A simple thought experiment suggests that the downward extension of a cyclonic vortex takes as long as it takes a parcel to descend through the layer with evaporational cooling. For a 4 km deep layer and a $0.1 ms^{-1}$ descent velocity, this time scale is 10 hours. However, in the control experiment, most of the evaporational cooling initially occurs well above the boundary layer. It takes several hours before the layer from 2-4 km moistens so that precipitation, and hence evaporation rates, increase at lower altitudes. The thought experiment also suggests that relative flow through the system could prevent development of a cyclone and its downward extension. It would seem that to get the needed vortex and its downward extension three things are important. First, precipitation has to last longer than it takes the parcels to descend through the layer of evaporation, to allow for the dispersion of the negative PV anomaly so that the positive anomaly dominates in the rain region. Second, in case of weak precipitation, the upper part of the lower troposphere has to be moistened so that the rain evaporation rates can increase closer to the surface. Third, relative flow through the system should be small. The first and third factor would also favor cyclogenesis owing to increased relative humidity.

The limitations of this work are mostly associated with the use of an axisymmetric model. The environment supposedly in radiative-convective equilibrium, with radiation and mean wind, cannot be simulated with an axisymmetric model. It is likely that in the presence of mean wind the extension of the cyclonic wind well into the boundary layer would play slightly less important role as it does in the absence of mean wind. More specifically, the reason that the simulation with showerhead lasting only 18 hours (HD) barely developed into a hurricane seemed to be at least partially owing to small cyclonic wind in the boundary layer at the time the showerhead was stopped (see Fig. 5.3c). At this time the

cold core did extend to the boundary layer (Fig. 5.3a), although in smaller region than at 22 h (Fig. 5.4a). In the presence of mean wind, the needed duration of the showerhead would probably be somewhat smaller than what the sensitivity studies suggest. Another question we could not answer is whether mean wind would prevent the vast increase of sea surface fluxes ahead of the outflow of low $\Theta_e$ air. Also the prediction of the thought experiment about the effect of shear, or more generally relative flow through the system, could not be tested with our axisymmetric model. Simulations with a three-dimensional model would be needed to learn more about the effect of relative flow through the system.

Many theoretical and numerical studies on tropical cyclogenesis have focused on the formation and/or intensification of a warm core vortex in the presence of convection. As RE and Emanuel (1989) show, downdrafts that bring air with low $\Theta_e$ to the boundary layer can prevent weak warm core vortices from developing into tropical cyclones. This is because $\Theta_e$ must have a positive anomaly in the boundary layer for convection to occur in a warm core vortex. This work suggests that initial disturbances with a lower tropospheric cold core may be less sensitive to the vertical advection of low $\Theta_e$ air, since convection can occur with lower values of boundary layer $\Theta_e$.

Many studies show that vorticity associated with convective systems is usually strongest in the middle troposphere, and there is often no positive anomaly of vorticity in the boundary layer. Consequently, a problem that has received a fair amount of attention is how these midlevel vortices can propagate to the lower troposphere. It is important to note that MCSs in environments with and without shear may be different. Many observational studies concern either squall lines or MCSs in the middle latitudes. Both are likely associated with larger shear than tropical non-squall mesoscale convective systems. Shear may explain why these case studies often show no vorticity extending to the boundary layer.

The simulations presented in Chapter 5 and the thought model show that the downward development occurs relatively fast in the absence of shear.

The composite study by Zehr (1976) shows that developing cloud clusters have a warm core inside a cold core in the lower troposphere, and nonintensifying cloud clusters have a cold core that does not extend to the top of the boundary layer. This supports the results presented in this thesis that the development of a cold core vortex and its downward propagation may often be key processes in tropical cyclogenesis.

It is interesting to note that to the author's knowledge the theory for tropical cyclogenesis outlined in this work is the first theory to explain why cyclogenesis is not well correlated with large-scale relative humidity (see McBride and Zehr 1981). In section 5.2 the sensitivity of the development of a hurricane, as resulting from evaporation of mesoscale precipitation, to large-scale relative humidity was tested. The results suggest that initially development is favored by dryness of the large-scale environment, but later development is favored by moist environment.

Based on this study, the intensity and duration of stratiform rain are of paramount importance for the development and the downward propagation of the vortex. In addition, the thought experiment suggest that a relative flow through the system may prevent the development and the downward propagation of the vortex. For the goal of understanding and forecasting tropical cyclogenesis, more should be learned about the formation and maintenance of MCSs. Even though there were no independent upper tropospheric PV anomalies in the region of pre-Guillermo (Molinari, personal communication 1996), it may be that in other cases of tropical cyclogenesis upper tropospheric PV anomalies could affect both the formation and maintenance of MCSs as well as the large-scale vertical shear.

# References


Anthes, R. A., 1972: Non-developing experiments with a three-level axisymmetric hurricane model. NOAA Tech. Memo. ERL NHRL-97, National Hurricane Research Laboratory, Coral Gables, FL, 18 pp.

Atlas, D., R. C. Srivastava, and R. S. Sekhon, 1973: Doppler radar characteristics of precipitation at vertical incidence. *Rev. Geophys. Space Phys.*, **11**, 1-35.

Avila, L., 1991: Atlantic tropical systems of 1990. *Mon. Wea. Rev.*, **119**, 2027-2033.

Bargen, D. W., and R. C. Brown, 1980: Interactive radar velocity unfolding. Preprints, *19th Conf. on Radar Meteor.*, Miami Beach, Amer. Meteor. Soc., 278-283.

Bartels, D. L., and R. A. Maddox, 1991: Midlevel cyclonic vortices generated by mesoscale convective systems. *Mon. Wea. Rev.*, **119**, 104-118.

Bosart, L. F., and F. Sanders, 1981: The Johnstown flood of July 1977: A long-lived convective system. *J. Atmos. Sci.*, **38**, 1616-1642.

Chen, S. S., and W. M. Frank, 1993: A numerical study of the genesis of extratropical convective mesovortices. Part I: Evolution and dynamics. *J. Atmos. Sci.*, **50**, 2401-2426.

Cotton, W. R., and R. A. Anthes. *Storm and Cloud Dynamics*, Academic Press, 1989, 883 pp.

Davidson, N. E., G. J. Holland, J. L. McBride, and T. D. Keenan, 1990: On the formation of AMEX cyclones Irma and Jason. *Mon. Wea. Rev.*, **118**, 1981-2000.

Davis, C. A., and M. L. Weisman, 1994: Balanced dynamics of mesoscale vortices produced in simulated convective systems. *J. Atmos. Sci.*, **51**, 2005-2030.

Elsberry, R. L., W. M. Frank, G. J. Holland, J. D. Jarrell, and R. L. Southern. *A Global View of Tropical Cyclones*, University of Chicago Press, 1987, 185 pp.

Emanuel, K. A., 1989: The finite amplitude nature of tropical cyclogenesis. *J. Atmos. Sci.*, **46**, 3432-3456.

Emanuel, K. A., 1991: TEXMEX Operations Plan., M.I.T.

Emanuel, K. A., 1995: The behavior of a simple hurricane model using a convective scheme based on subcloud-layer entropy equilibrium. *J. Atmos. Sci.*, **52**, 3960-3968.

Emanuel, K. A., J. D. Neelin, and C. S. Bretherton, 1994: On large-scale circulations in convecting atmospheres. *Quart. J. Roy. Meteor. Soc.*, **120**, 1111-1143.

Farfan, L. M., and J. A. Zehnder, 1996: Synoptic and mesoscale circulations associated with the genesis of hurricane Guillermo (1991). Submitted to *Mon. Wea. Rev.*

Fjørtoft, R., 1953: On the changes in the spectral distribution of kinetic energy for two-dimensional, nondivergent flow. *Tellus*, **5**, 225-230.

Gamache, J. F., and R. A. Houze, Jr., 1982: Mesoscale air motions associated with a tropical squall line. *Mon. Wea. Rev.*, **110**, 118-135.

Gamache, J. F., and R. A. Houze, Jr., 1985: Further analysis of the composite wind and thermodynamic structure of the 12 September GATE squall line. *Mon. Wea. Rev.*, **113**, 1241-1259.

Gray, W. M., 1968: Global view of the origin of tropical disturbances and storms. *Mon. Wea. Rev.*, **96**, 669-700.

Handel, M. D., 1990: *Tropical cyclone intensification from finite amplitude disturbances or how hurricanes hardly happen.* Ph.D. thesis, Massachusetts Institute of Technology, Cambridge, Massachusetts, 261 pp.

Hawkins, H. F., and S. M. Imbembo, 1976: The structure of a small, intense hurricane, Inez 1966. *Mon. Wea. Rev.*, **104**, 418-442.

Hoskins, B. J., M. E. McIntyre, and A.W. Robertson, 1985: On the use and significance of isentropic potential vorticity maps. *Quart. J. Roy. Meteor. Soc.*, **111**, 877-946.

Houze, R. A., Jr., *Cloud Dynamics.* Academic Press, 1993, 573 pp.

Jones, S. C., 1995: The evolution of vortices in vertical shear. I: Initially barotropic vortices. *Quart. J. Roy. Meteor. Soc.*, **121**, 821-851.

Jordan, C. L., 1958: Mean soundings for the West Indies area. *J. Meteor.*, **15**, 91-97.

Jorgensen, D. P., P. H. Hildebrandt, and C. L. Frush, 1983: Feasibility test of an airborne pulse-Doppler meteorological radar. *J. Climate Appl. Meteor.*, **22**, 744-757.

Joss, J., and A. Waldvogel, 1970: Raindrop size distribution and Doppler velocities. Preprints, *14th Conf. on Radar Meteor.*, Tuscon, Amer. Meteor. Soc., 153-156.

Kessler, E., 1969: *On the Distribution and Continuity of Water Substance in Atmospheric Circulation.* Meteor. Monogr., No. 32, Amer. Meteor. Soc., 84 pp.

Klemp, J. B., and R. B. Wilhelmson, 1978: The simulation of three-dimensional convective storm dynamics. *J. Atmos. Sci.*, **35**, 1070-1096.

Kundu, P. K., *Fluid Mechanics.* Academic Press, 1990, 638 pp.

Laing A. G., and J. M. Fritsch, 1993: Mesoscale convective complexes in Africa. *Mon. Wea. Rev.*, **121**, 2254-2263.

Lilly, D. K., 1962: On the numerical simulation of buoyant convection. *Tellus*, **14**, 148-172.

Lindzen, R. S., *Dynamics in Atmospheric Physics.* Cambridge University Press,1990, 310 pp.

Mapes, B. E., and R. A. Houze Jr., 1995: Diabatic divergence profiles in western Pacific mesoscale convective systems. *J. Atmos. Sci.*, **52**, 1807-1828.

Marks, F. D., and R. A. Houze, 1984: Airborne Doppler radar observations in hurricane Debby. *Bull. Amer. Meteor. Soc.*, **65**, 569-582.

Marks, F. D., and R. A. Houze, 1987: Inner core structure of hurricane Alicia from airborne Doppler radar observations. *J. Atmos. Sci.*, **44**, 1296-1317.

Mason, P. J., and R. I. Sykes, 1982: A two-dimensional numerical study of horizontal roll vortices in an inversion capped planetary boundary layer. *Quart. J. Roy. Meteor. Soc.*, **108**, 801-823.

McBride, J. L., and R. Zehr, 1981: Observational analysis of tropical cyclone formation. Part II: Comparison of non-developing versus developing systems. *J. Atmos. Sci.*, **38**, 1132-1151.

Merceret, F. J., and H. W. Davis, 1981: T*he determination of navigational and meteorological variables measured by NOAA/RFC WP3D aircraft.* NOAA Tech. Memo ERL RFC-7, Miami, Florida, 25 pp.

Miller, R. J., 1991: Tropical cyclogenesis in the eastern North Pacific from an African wave. Preprints, *19th Conf. on Hurricanes and Tropical Meteor.*, Miami, Amer. Meteor. Soc., 245-248.

Molinari, J., S. Skubis, and D. Vollaro, 1995: External influences on hurricane intensity. Part III: Potential vorticity structure. *J. Atmos. Sci.*, **52**, 3593-3606.

Montgomery, M. T., and B. F. Farrell, 1993: Tropical cyclone formation. *J. Atmos. Sci.*, **50**, 285 - 310.

Moss, M. S., and S. L. Rosenthal, 1975: On the estimation of planetary boundary layer variables in mature hurricanes. *Mon. Wea. Rev.*, **103**, 980-988.

Newell, R. E., J. W. Kidson, D. G. Vincent, and G. J. Boer, 1972. *The General Circulation of the Tropical Atmosphere and Interactions with Extratropical Latitudes*, Vol. 1. Cambridge, MA, M.I.T. Press.

Ogura, Y., and T. Takahashi, 1971: Numerical simulation of the life cycle of a thunderstorm cell. *Mon. Wea. Rev.*, **99**, 895 -911.

Reilly, D. H., 1992: *On the role of upper-tropospheric potential vorticity advection in tropical cyclone formation: Case studies from 1991.* M. Sc. thesis, Massachusetts Institute of Technology, Cambridge, Massachusetts, 124 pp.

Riehl, H., *Tropical meteorology*. McGraw-Hill Book Co., 1954, 392 pp.

Rennó, N., L. R. Schade, M. C. Morgan, M. Bister, C.-C. Wu, and D. Reilly, 1992: *Tropical Experiment in Mexico: Data report.* Available from K. A. Emanuel, M.I.T.

Rogers, R. R., and M. K. Yau. *A short course in cloud physics.* Pergamon Press, 1989, 293 pp.

Rotunno, R., and K. A. Emanuel, 1987: An air-sea interaction theory for tropical cyclones. Part II: Evolutionary study using a nonhydrostatic axisymmetric numerical model. *J. Atmos. Sci.*, **44**, 542-561.

Shapiro, L. J., 1977: Tropical storm formation from easterly waves: A criterion for development. *J. Atmos. Sci.*, **34**, 1007-1021.

Simpson, R. H., and H. Riehl. *The hurricane and its impact.* Louisiana State University Press, 1981, 398 pp.

Soong, S.-T., and Y. Ogura, 1973: A comparison between axisymmetric and slab-symmetric cumulus cloud models. *J. Atmos. Sci.*, **30**, 879 - 893.

Velasco I., and J. M. Fritsch, 1987: Mesoscale convective complexes in the Americas. *J. Geophys. Res.*, **92**, 9591-9613.

Yamasaki, M., 1977: A preliminary experiment of the tropical cyclone without parameterizing the effects of cumulus convection. *J. Meteor. Soc. Japan*, **55**, 11-31.

Zehnder J. A., and R. L. Gall, 1991: On a mechanism for orographic triggering of tropical cyclones in the Eastern North Pacific. *Tellus*, **43A**, 25-36.

Zehr, R., 1976: *Tropical disturbance intensification.* Dept. of Atmos. Sci. Pap. No. 259, Colorado State University, 91 pp.

Zehr, R., 1992: *Tropical cyclogenesis in the western north Pacific.* NOAA Tech. Report NESDIS-61, 163 pp.

6213-17